Universal asymptotic correlation functions for point group C_{6v} and an observation for triangular lattice Q-state Potts model

Masafumi Fujimoto [1] and Hiromi Otsuka [2]
[1]*Department of Physics, Nara Medical University, Kashihara, Nara 634-8521, Japan*
[2]*Department of Physics, Tokyo Metropolitan University, Hachioji, Tokyo 192-0397, Japan*

(Received 4 August 2022; accepted 24 January 2023; published 13 February 2023)

We investigate a universal curve in asymptotic correlation functions of off-critical systems that possess C_{6v} symmetry following the argument for C_{4v} symmetry in our previous paper [Phys. Rev. E **102**, 032141 (2020)]. Unlike the C_{4v} case, a minimal asymptotic form exists, which contains only two free parameters: the normalization constant and the modulus of the universal curve. We perform large-scale Monte Carlo simulations of the triangular lattice Q-state Potts model above the transition temperature. For $Q = 1$, 2, 3, and 4, we successfully obtain numerical evidence that the minimal form gives the leading asymptotic behavior. We also discuss the possibility that the corrections to the minimal form are expressed using this form as a building block. From the minimal form with optimized parameters, we derive the equilibrium crystal shape of the honeycomb lattice Potts model, which is given by an algebraic curve of genus 1 and is universal among models with C_{6v}. Although the curve differs from those obtained in the C_{4v} case, the latter curves also have genus 1. We indicate that the birational equivalence concept can play an important role in comparing asymptotic forms for different point group symmetries, for example, C_{6v} and C_{4v}.

DOI: 10.1103/PhysRevE.107.024118

I. INTRODUCTION

The thermal evolution of the equilibrium crystal shape (ECS) is a long-standing problem. In 1901, Wulff [1] proposed a method to determine the ECS from the anisotropic interfacial tension, which is called Wulff's construction; also see Refs. [2,3]. ECSs are polygons or polyhedrons at the zero-temperature limit. When the interactions are isotropic, they become circles or spheres near the critical temperature. A roughening transition exists between them [4].

The roughening transition should be investigated as a cooperative phenomenon from the microscopic Hamiltonian within the framework of statistical mechanics. Practically, however, it is quite difficult for these calculations to give reliable results. In the 1970s, the development of exact analyses of solvable lattice models enabled detailed studies of the roughening transition. In the early stage of research, the disappearance of a sharply defined interface at the roughening transition temperature T_{R} received much attention. In Refs. [5,6], the interface profile of the square lattice Ising model was investigated to show that its width diverges at the thermodynamic limit. Then, it was recognized that this phase transition might influence crystal morphology [7–11]. Pioneering research on this issue was conducted in Refs. [7,8], where the body-centered solid-on-solid (BCSOS) model was investigated with the help of the exact solutions of the six-vertex model [12,13]. The facet shape in the BCSOS model was analyzed to identify a universal jump at T_{R} in the principal curvature of the two-dimensional (2D) surface of the three-dimensional ECS; also see Refs. [14,15]. Meanwhile, for the square lattice Ising model, the 2D ECS was calculated in Refs. [9–11] and expressed as a simple algebraic curve in the $\alpha\beta$ plane:

$$\alpha^2\beta^2 + 1 + A_3(\alpha^2 + \beta^2) + A_4\alpha\beta = 0, \tag{1.1}$$

with $\alpha = \exp[-\lambda(X + Y)/k_{\mathrm{B}}T]$ and $\beta = \exp[-\lambda(X - Y)/k_{\mathrm{B}}T]$, where (X, Y) is the position vector of a point on the ECS and λ is a scale factor; for the definitions of A_3 and A_4, see Ref. [11].

In Ref. [16], the authors indicated that the ECS (1.1) is identical to the facet shape of the BCSOS model. The accumulation of research on the ECSs revealed a paradoxical scenario: Clearly, the interfaces of lattice models have model-dependent microscopic profiles (see, e.g., Ref. [17]). Equation (1.1) commonly represents the ECSs of a wide range of solvable models [18–20]. Furthermore, for some unsolvable models, researchers showed that the ECS (or facet shape) is quite close to Eq. (1.1) [21–23].

For the square lattice Ising model, the anisotropic correlation length (ACL) is related by duality to the anisotropic interfacial tension [24]. The ECS (1.1) was derived from the ACL via the duality relation and Wulff's construction; also see Refs. [16,25,26]. Thus, Eq. (1.1) appears in the representation of the asymptotic correlation function of the square lattice Ising model. The same situation was found in other solvable models on the square lattice without the duality relation [18,19]. These facts suggested a close relationship between the algebraic curve (1.1) and symmetry properties of the square lattice; see, for example, Ref. [27].

Quite recently, Fujimoto and Otsuka [28] investigated the asymptotic correlation functions of the square lattice Q-state Potts model. The model is solvable at the phase transition point [13,29–31]. For $Q > 4$, the phase transition is first order.

TABLE I. The first column shows the elements in C_{2v}: π-rotation c_2, vertical reflection σ_x, and horizontal reflection σ_y; the second shows the corresponding coordinate transformations; and the third shows the induced transformations of the integration path in Eq. (2.1). Conditions in the fourth column are required for $\mathcal{X}(\Theta)$ and $\mathcal{Y}(\Theta)$ to ensure C_{2v} symmetry.

C_{2v}	Coordinate trans.	Path shifts	Conditions for $\mathcal{X}(\Theta)$ and $\mathcal{Y}(\Theta)$
c_2	$(n', m') = (-n, -m)$	$\Theta' = \Theta + \omega_2$	$\mathcal{X}(\Theta') = \mathcal{X}(\Theta)^{-1}$, $\mathcal{Y}(\Theta') = \mathcal{Y}(\Theta)^{-1}$
σ_x	$(n', m') = (n, -m)$	$\Theta' = -\Theta$	$\mathcal{X}(\Theta') = \mathcal{X}(\Theta)$, $\mathcal{Y}(\Theta') = \mathcal{Y}(\Theta)^{-1}$
σ_y	$(n', m') = (-n, m)$	$\Theta' = -\Theta + \omega_2$	$\mathcal{X}(\Theta') = \mathcal{X}(\Theta)^{-1}$, $\mathcal{Y}(\Theta') = \mathcal{Y}(\Theta)$

Researchers showed that Eq. (1.1) appears in the asymptotic behavior of the correlation function at the first-order transition point [20]; also see Refs. [32,33]. When $Q = 2$, the Potts model reduces to the Ising model. We reexamined its asymptotic correlation function both above and below the transition temperature. Using the combination of the transfer matrix and shift operator [18,34–36], we reproduced the same results as those using the Pfaffian method [37,38]; also see Refs. [39–42]. Furthermore, we analyzed the Ising model on a square lattice rotated through an arbitrary angle with respect to the coordinate axes. Johnson, Krinsky, and McCoy [43] showed that the summation over the eigenvalues of the transfer matrix becomes contour integrals in the thermodynamic limit. Although lattice rotation causes the integration paths to move, the contour integrals must be independent of the path movement. We found that (i) wide analyticity domains of the eigenvalues of the transfer matrix and the shift operator is necessary to ensure path independence with the help of Cauchy's theorem; (ii) satisfying a functional equation corresponds to π-rotational invariance; and because 2π rotation returns the contour integrals to the original integrals, (iii) the eigenvalues possess doubly periodic structures.

We pointed out a possibility that (i)–(iii) are connected with C_{2v} symmetry, not with the exact solvability of the Ising model; hence, they apply to a general Q. Assuming a massive dispersion curve, and using these properties, we can construct the general asymptotic form Eq. (2.1) with Eq. (2.2) in Ref. [28]. The system possesses C_{4v} symmetry when the interactions are isotropic. Because C_{2v} is a normal subgroup of C_{4v}, we found Eq. (2.3) [or equivalently Eq. (3.2)] in Ref. [28], which contains three free parameters. To test Eq. (3.2), we numerically analyzed correlation function data provided by Monte Carlo (MC) simulations. Choosing the three parameters suitably, we reproduced the MC data over wide areas with high accuracy; see Table I of Ref. [28]. Thus, we obtained strong evidence that the asymptotic form Eq. (3.2) in Ref. [28] applies to the correlation function and the ACL in the disordered phase.

From C_{4v} symmetry the shape in Eq. (1.1) possibly deforms for general Q. In Eq. (3.2) of Ref. [28], one of the free parameters corresponding to the deformations was denoted by b. We derived the ECSs via duality [20,44] and Wulff's construction. Then, we found that Eq. (1.1) should be replaced by

$$\alpha^2\beta^2 + 1 + \bar{A}_2(\alpha\beta + 1)(\alpha + \beta) + \alpha^2 + \beta^2 + \bar{A}_4\alpha\beta = 0 \tag{1.2}$$

(also see Sec. IV B and Ref. [45]). We numerically detected a quite small Q dependence of the ECSs: For $Q = 2$, $b = 1$, that is, an exact value, where Eq. (1.2) is reduced to Eq. (1.1) [45]. The MC data showed that $b > 1$ for $Q = 1$ (the bond percolation), and $b < 1$ for $Q = 3, 4$. According to Eq. (1.2), the ECS is rounded in the facet directions and flattened in the corner directions as Q increases.

The results in Ref. [28] strongly suggest that the three properties (i)–(iii) connect with the C_{2v} symmetry. Analysis for C_{6v} is desirable since C_{6v} also contains C_{2v} as a normal subgroup. From the viewpoint of solvability structures, the study of the C_{6v} cases is quite interesting. Some attempts have been made to calculate the asymptotic correlation functions on the triangular lattice Ising model by the Pfaffian method [46]; also see Refs. [47,48], Chap. VIII of Ref. [38], and Ref. [49]. In Ref. [26], the analyses were extended for Ising models on honeycomb, diced, and Kagomé lattices. Little is known about transfer matrices for these models. However, the asymptotic form in the Kagomé lattice eight-vertex model [50] and that of the triangular/honeycomb lattice Potts model at the first-order transition point [51] were calculated using the transfer matrix argument. Unlike the square lattice case, however, the commuting transfer matrices can only be constructed along some special directions for these lattices.

In this paper, following the analysis for the C_{4v} case [28], we consider asymptotic correlation functions with C_{6v} symmetry. Our strategy for investigating the C_{6v} symmetric case is as follows: We expect that the transfer matrices satisfy the three properties (i)–(iii) mentioned above. This leads us to the asymptotic correlation function given by Eq. (2.1) with Eq. (2.2) in Ref. [28]. The factor group C_{4v}/C_{2v} is the cyclic group of order 2. However, the factor group C_{6v}/C_{2v} is the cyclic group of order 3. We find a minimal form that includes only two parameters. This is because one more condition than that for C_{4v} fixes the b parameter and then yields a model-independent minimal form for C_{6v}. Although the number of free parameters, two, is equal to that in the usual Ornstein–Zernike (OZ) form, our minimal form possesses discrete C_{6v} symmetry.

To proffer numerical evidence to support the applicability of the minimal form with C_{6v}, we perform large-scale MC simulations of the triangular lattice Q-state Potts model [13,31]. We analyze the MC data of the asymptotic correlation functions for the $Q = 1$, 2, 3, and 4 cases above the critical temperature. We find that the minimal form well fits numerical data in these cases and yields precise estimates of the ACLs. Additionally, we fit the data using the OZ form and reveal the superiority of the minimal form via a comparison of their fittings.

We present some implications of our findings for asymptotic correlation functions on the triangular lattice. Unlike the case of C_{4v}, ACLs include only one parameter: the modulus.

This fact means that, in discussing long-distance behavior, Potts models with various Q have the same character, with a mere rescaling of the temperature. Using the ACLs obtained from the minimal form, we derive the ECS on the honeycomb lattice via the duality transformation and Wulff's construction, which suggests that the same asymptotic forms appear in the honeycomb lattice Potts model. Furthermore, similar to the case of C_{4v} symmetry, the ECS is given by an algebraic curve of genus 1. Based on the previous study [28] and the present study, we can explain the mathematical background to relate the asymptotic correlation functions of different models, even on different 2D lattices.

The present paper is organized as follows: In Sec. II, we provide the minimal form adaptable to asymptotic correlation functions with C_{6v} symmetry. In Sec. III, we perform MC simulations of the triangular lattice Q-state Potts model in disordered phases. The minimal form fits the numerical data of correlation functions well and yields precise estimates of the ACLs. Additionally, we fit data using the OZ form and reveal the superiority of the minimal form by comparing their fittings. In Sec. IV, we discuss and summarize the study. We derive an ECS on the honeycomb lattice from the ACLs in triangular lattice models. Then we provide a birational transformation [52] to connect the algebraic curve for C_{6v} to that for C_{4v}. In Appendices A and B, we explain the exact calculation of the asymptotic correlation function of the triangular lattice Ising model by the transfer matrix method and derive the birational transformation given in Sec. IV, respectively.

II. ASYMPTOTIC CORRELATION FUNCTIONS FOR C_{6v}

To make our discussion specific, we assume a triangular lattice on which the Q-state Potts model with isotropic interactions is defined. In Ref. [28], from the exact calculation of the $Q = 2$ Potts model on a square lattice, it was explicitly shown that the three properties (i)–(iii) are satisfied; see also [53]. Here we derive general forms of the correlation functions with C_{6v} symmetry using them as necessary basic conditions.

As depicted in Fig. 1, a triangular lattice consists of all points with position vectors $\mathbf{r} = j\mathbf{a}_1 + i\mathbf{a}_2$, where the primitive vectors are denoted by $\mathbf{a}_1$ and $\mathbf{a}_2$. The lattice spacing $|\mathbf{a}_1| = |\mathbf{a}_2| = a$ and the angle between them is $2\pi/3$. For the triangular lattice Ising model, the asymptotic correlation function was analyzed using the Pfaffian method [46]; also see Refs. [26,49]. We can derive almost the same results by introducing the shift operator into the transfer matrix method. We restrict ourselves to the case of isotropic interactions, where the system possesses C_{6v} symmetry. To find the role of C_{6v} symmetry, we investigate the model on triangular lattices rotated clockwise through various angles to the coordinate axes: we consider the cases of the rotation angle $n\pi/6$ with $n = 0, 1, \ldots, 11$. We summarize the main results in the main text and provide the details in Appendix A.

In the thermodynamic limit, the summations over eigenvalues of the transfer matrix and of the shift operator become integrals because of their continuous distribution. The asymptotic correlation functions are represented using contour integrals on Riemann surfaces, as shown in Eqs. (A9) and (A12); also see Refs. [13,43]. Considering transfer matrices in the rotated systems shows that the three properties (i)–(iii) are

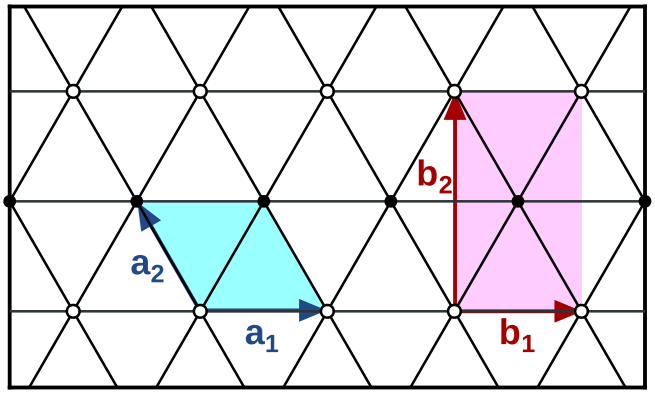

FIG. 1. Blue arrows $\mathbf{a}_1$ and $\mathbf{a}_2$ represent the primitive vectors of the triangular lattice, which correspond to $\mathcal{A}_1(\Theta)$ and $\mathcal{A}_2(\Theta)$ in Eq. (2.7), respectively. We divide the triangular lattice into two sublattices, represented by open and closed circles. Red arrows $\mathbf{b}_1$ and $\mathbf{b}_2$ represent the primitive vectors of a sublattice, which correspond to $\mathcal{X}(\Theta)$ and $\mathcal{Y}(\Theta)$ in Eq. (2.1), respectively.

fulfilled: In Appendix A 2, we indicate that the lattice rotations shift the integration paths for $Q = 2$. After the eigenvalues are summed up, thermodynamic averages must be independent of the rotation angle. This equivalence is derived with the help of the analyticity of the eigenvalues of the transfer matrices and the shift operators. Hence, (i) wide analyticity domains of the eigenvalues is indispensable; (ii) the eigenvalues should satisfy a functional equation corresponding to the π-rotational symmetry; see Eq. (A27) or Eq. (A28) in Ref. [28]; and (iii) the eigenvalues should possess two periods. Intuitively, we can explain this property as follows: The 2D lattice models are related to the 2D Euclidean field theories in their critical limit and for distances much larger than a. The correlation function has the periodicity of rotational symmetry in the limit. For off-critical lattice models, the crystal momentum is defined as modulo $2\pi/a$. Therefore, any lattice models possess two types of periodicity: one is the two, four, or sixfold rotational symmetry, and the other is that the eigenvalues of transfer matrices are periodic functions of the crystal momentum.

Because C_{2v} is the normal subgroup of C_{6v}, we consider C_{2v} symmetry as the first step; that is, we start with (i)–(iii) to shape the asymptotic correlation functions with C_{6v} symmetry. For this purpose, it is convenient to divide the triangular lattice into two sublattices shown by open and closed circles in Fig. 1. Let $\mathbf{o}$ be the position vector of the origin, and $\mathbf{r}^+$ that of another site in the same sublattice. Then, in terms of the primitive vectors of sublattice $\mathbf{b}_1$ and $\mathbf{b}_2$, $\mathbf{r}^+ = n\mathbf{b}_1 + m\mathbf{b}_2 = (n+m)\mathbf{a}_1 + 2m\mathbf{a}_2$. We suppose a massive dispersion curve. The above-mentioned situation is expected to occur for general Q: The thermodynamic averages are represented in terms of contour integrals on Riemann surfaces. Although lattice rotations make integration paths move, they are independent of the rotation angle. To ensure the independency and C_{2v} symmetry, (i)–(iii) are expected to be satisfied.

Because of property (iii), the massive dispersion curve can be parametrized in terms of elliptic functions; the argument is denoted by Θ, and the half periods are by ω_1 and ω_1. We can represent the leading asymptotic correlation function between $\mathbf{o}$ and $\mathbf{r}^+$ as a contour integral on a Riemann surface of genus

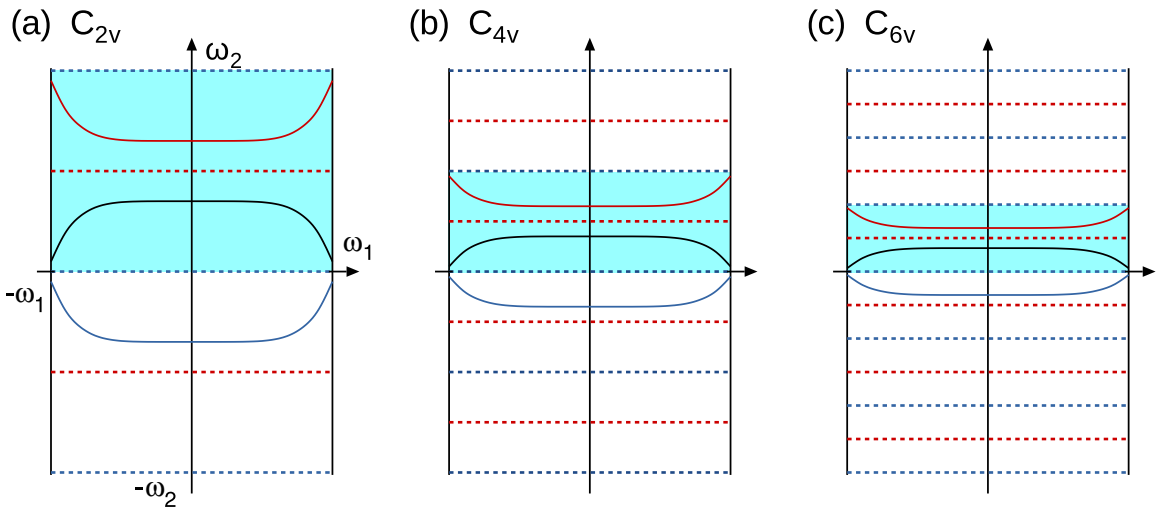

FIG. 2. Periodic rectangles for (a) C_{2v}, (b) C_{4v}, and (c) C_{6v}. They are divided into (a) two, (b) four, and (c) six subregions because of the rotational symmetries; a cyan area represents a subregion. Blue and red dotted lines are the reflection axes for the integration paths (see the text). For instance, (a) integrals along the paths represented by the black, blue, and red curves yield the same result for Eq. (2.1) if m and n are transformed correspondingly. The same occurs (b) in Eq. (2.3) in Ref. [28] for C_{4v}, and (c) in Eq. (2.6) for C_{6v}.

1 (see Fig. 2):

$$\mathcal{F}_{\mathbf{o},\mathbf{r}^+} \sim \int_{-\omega_1}^{\omega_1} d\Theta\, \rho(\Theta)\mathcal{X}(\Theta)^n\mathcal{Y}(\Theta)^m, \tag{2.1}$$

where $\mathcal{Y}(\Theta)$ corresponds to eigenvalues of the row-to-row transfer matrix along the vertical direction and $\mathcal{X}(\Theta)$ to those of the shift operator along the horizontal direction; $\rho(\Theta)$ is to be determined from the distribution of the eigenvalues and the matrix elements. We assume that the ACL is obtainable from Eq. (2.1) by the saddle-point method; see Sec. IV A. Then, as discussed below Eq. (A10) in Appendix A, we expect that $\rho(\Theta) = \text{const}$.

As explained above, $\mathcal{X}(\Theta)$ and $\mathcal{Y}(\Theta)$ are doubly periodic functions: $\mathcal{X}(\Theta + 2\omega_1) = \mathcal{X}(\Theta + 2\omega_2) = \mathcal{X}(\Theta)$ and $\mathcal{Y}(\Theta + 2\omega_1) = \mathcal{Y}(\Theta + 2\omega_2) = \mathcal{Y}(\Theta)$. Also the property (ii), the invariance under π-rotation (say c_2), enforces the functional equations among them:

$$\mathcal{X}(\Theta + \omega_2) = \mathcal{X}(\Theta)^{-1}, \quad \mathcal{Y}(\Theta + \omega_2) = \mathcal{Y}(\Theta)^{-1}. \tag{2.2}$$

From C_{2v} symmetry, it follows that (i) analytic regions of $\mathcal{X}(\Theta)$ and $1/\mathcal{X}(\Theta)$ must appear alternatively along the ω_2 direction; and the same is true for $\mathcal{Y}(\Theta)$ and $1/\mathcal{Y}(\Theta)$; thus $\mathcal{X}(\Theta)$ and $\mathcal{Y}(\Theta)$ are meromorphic functions. Using their series expansions, we obtain

$$\mathcal{X}(\Theta) = \prod_{l=1}^{v} k^{\frac{1}{2}}\,\mathrm{sn}(\Theta + \alpha_l), \quad \mathcal{Y}(\Theta) = \prod_{l=1}^{v'} k^{\frac{1}{2}}\,\mathrm{sn}(\Theta + v + \beta_l), \tag{2.3}$$

where $k \in (0, 1)$ is the modulus corresponding to the modular parameter $\tau = \omega_2/\omega_1$; see Appendix A.3 of Ref. [28]. For definitions of Jacobi's elliptic functions, see Chap. 15 of Ref. [13].

In addition to c_2, it is necessary to consider the invariance of Eq. (2.1) under the vertical reflection (σ_x) or the horizontal reflection (σ_y) to achieve C_{2v} symmetry. For example, we obtain the following functional equations from the invariance under σ_x:

$$\mathcal{X}(-\Theta) = \mathcal{X}(\Theta), \quad \mathcal{Y}(-\Theta) = \mathcal{Y}(\Theta)^{-1}. \tag{2.4}$$

Because $\sigma_y = \sigma_x \cdot c_2$, the conditions (2.2) and (2.4) yield the invariance of Eq. (2.1) under σ_y. In Table I, we summarize the functional equations to achieve C_{2v} symmetry. Because $\mathrm{sn}(-\Theta) = -\mathrm{sn}(\Theta)$, we find that $v = -\omega_2/2$, and v and v' are even integers. Additionally, τ must be purely imaginary because the correlation function is real-valued (see below).

Note that c_2 shifts integration paths by ω_2 without deforming them. In this sense, twofold rotational symmetry divides a periodic rectangle into two subregions. Meanwhile, the reflections σ_x and σ_y cause reflections of paths about the blue and red dotted lines in Fig. 2(a), respectively. Consequently, the equivalent integration paths appear repeatedly in the periodic rectangle because of C_{2v} symmetry.

We showed in Ref. [28] that to derive the asymptotic forms for C_{4v} from those for C_{2v}, fourfold rotational symmetry requires an additional functional equation: $\mathcal{Y}(\Theta) = \mathcal{X}(\Theta - \omega_2/2)$ (see the upper part of Table II). Similarly, we construct an asymptotic form for C_{6v} from those for C_{2v}. For this aim, it is convenient to introduce $\mathcal{A}_1(\Theta)$ and $\mathcal{A}_2(\Theta)$. These are associated with primitive translations of $\mathbf{a}_1$ and $\mathbf{a}_2$, respectively, and are related to $\mathcal{X}(\Theta)$ and $\mathcal{Y}(\Theta)$ as

$$\mathcal{X}(\Theta) = \mathcal{A}_1(\Theta), \quad \mathcal{Y}(\Theta) = \mathcal{A}_2(\Theta)^2\mathcal{A}_1(\Theta) \tag{2.5}$$

(see Fig. 1). Then, sixfold rotational symmetry yields two additional functional equations:

$$\mathcal{A}_2(\Theta) = \mathcal{A}_1\left(\Theta - \frac{2\omega_2}{3}\right), \quad \mathcal{A}_1(\Theta)\mathcal{A}_2(\Theta) = \mathcal{A}_1\left(\Theta - \frac{\omega_2}{3}\right) \tag{2.6}$$

(see the lower part of Table II). Using $\mathcal{A}_1(\Theta)$ and $\mathcal{A}_2(\Theta)$, we can express the correlation function between $\mathbf{o}$ and $\mathbf{r} = j\mathbf{a}_1 + i\mathbf{a}_2$ as

$$\mathcal{F}_{\mathbf{o},\mathbf{r}} \sim \text{const} \int_{-\omega_1}^{\omega_1} d\Theta\, \mathcal{A}_1(\Theta)^j\mathcal{A}_2(\Theta)^i. \tag{2.7}$$

TABLE II. Conditions for C_{4v} and C_{6v} in addition to those for C_{2v} in Table I. In the C_{4v} case, invariance under $\pi/2$-rotation c_4 imposes one more condition between $\mathcal{X}(\Theta)$ and $\mathcal{Y}(\Theta)$. In the C_{6v} case, invariance under $\pi/3$-rotation c_6 and $2\pi/3$-rotation c_6^2 require two more conditions between $\mathcal{A}_1(\Theta)$ and $\mathcal{A}_2(\Theta)$.

C_{4v}	Coordinate trans.	Path shifts	Condition for $\mathcal{X}(\Theta)$ and $\mathcal{Y}(\Theta)$
c_4	$(n', m') = (-m, n)$	$\Theta' = \Theta + \frac{\omega_2}{2}$	$\mathcal{Y}(\Theta') = \mathcal{X}(\Theta)$
C_{6v}	Coordinate trans.	Path shifts	Conditions for $\mathcal{A}_1(\Theta)$ and $\mathcal{A}_2(\Theta)$
c_6	$(j', i') = (j - i, j)$	$\Theta' = \Theta + \frac{\omega_2}{3}$	$\mathcal{A}_1(\Theta')\mathcal{A}_2(\Theta') = \mathcal{A}_1(\Theta)$
c_6^2	$(j', i') = (-i, j - i)$	$\Theta' = \Theta + \frac{2\omega_2}{3}$	$\mathcal{A}_2(\Theta') = \mathcal{A}_1(\Theta)$

A. Minimal case for C_{6v}

The unit cell of a sublattice is vertically long (see Fig. 1), and the relations (2.5) and (2.6) require a condition for the integers: $\nu' = 2\nu$. Therefore, we can find the simplest expression by setting $\nu = 2$ and $\nu' = 4$ in Eq. (2.3), whose parameters are fixed as $\alpha_1 = -\alpha_2 = \omega_2/6$, $\beta_1 = \beta_2 = 0$, and $\beta_3 = -\beta_4 = \omega_2/3$. The integrand is built from two elliptic functions, each composed of two sn functions, and possesses essentially the same structure as the simplest case for C_{4v} [28]. As different points, we replace the value of $\omega_2/2$ in Eq. (2.3) in Ref. [28] with $2\omega_2/3$ and fix the undetermined constant B to $\omega_2/6$ because C_{6v} requires not one but two additional conditions, as given in Table II.

As a result, a minimal form of the asymptotic correlation function with C_{6v} symmetry is obtained as

$$\mathcal{F}^{(\mathrm{min})}_{\mathbf{o},\mathbf{r}} = \mathrm{const} \int_{-\omega_1}^{\omega_1} d\Theta \left[k\,\mathrm{sn}\left(\Theta + \frac{\omega_2}{6}\right)\mathrm{sn}\left(\Theta - \frac{\omega_2}{6}\right)\right]^j \times \left[k\,\mathrm{sn}\left(\Theta - \frac{\omega_2}{2}\right)\mathrm{sn}\left(\Theta - \frac{5\omega_2}{6}\right)\right]^i. \tag{2.8}$$

Note that Eq. (2.8) contains only two parameters: a normalization constant and modulus k.

Once we determine the expressions of these parameters as Eqs. (A10) and (A11), Eq. (2.8) provides the leading asymptotic correlation function of the triangular lattice Ising model above the critical temperature. Because the pair of integers $(\nu, \nu') = (2, 4)$ cannot change as a result of continuous variations of Q, the minimal case applies unless a phase transition occurs. Indeed, we found that the simplest case with $\nu = \nu' = 2$ is commonly observed in the square lattice Q-state Potts model in the disordered phase [28]. Therefore, we expect that the minimal form (2.8), including the normalization factor and modulus as free parameters, describes the leading asymptotic behavior of the triangular lattice Q-state Potts model above the transition temperature $T_{\mathrm{C}}(Q)$ [see Eq. (3.2)].

B. Next to minimal case

We find a candidate of the next to the minimal case by setting $(\nu, \nu') = (4, 8)$ in Eq. (2.3). In addition to α_1, α_2, $\beta_1, \ldots \beta_4$, six parameters exist; say $\bar{\alpha}_1$, $\bar{\alpha}_2$, $\bar{\beta}_1$, $\ldots \bar{\beta}_4$. We introduce Θ for α_is and β_js, and $\bar{\Theta}$ for $\bar{\alpha}_i$s and $\bar{\beta}_j$s. The contour integral in Eq. (2.1) is replaced by a double integral with respect to Θ and $\bar{\Theta}$, and $\rho(\Theta)$ by $\rho(\Theta, \bar{\Theta})$. Suppose that their ACLs can be calculated by the method of steepest descent. Then, we find $\rho(\Theta, \bar{\Theta}) = \rho(\Theta - \bar{\Theta})$; see the argument below Eq. (A13) in Appendix A. To determine the asymptotic form, we repeat the same argument as that in the previous subsection. Then, we obtain a form for the next to the minimal case as follows:

$$\mathcal{F}^{(\mathrm{next})}_{\mathbf{o},\mathbf{r}} = \int_{-\omega_1}^{\omega_1} d\Theta \int_{-\omega_1}^{\omega_1} d\bar{\Theta}\, \rho(\Theta - \bar{\Theta}) \left[k\,\mathrm{sn}\left(\Theta + \frac{\omega_2}{6}\right)\mathrm{sn}\left(\Theta - \frac{\omega_2}{6}\right)\right]^j \left[k\,\mathrm{sn}\left(\Theta - \frac{\omega_2}{2}\right)\mathrm{sn}\left(\Theta - \frac{5\omega_2}{6}\right)\right]^i \times \left[k\,\mathrm{sn}\left(\bar{\Theta} + \frac{\omega_2}{6}\right)\mathrm{sn}\left(\bar{\Theta} - \frac{\omega_2}{6}\right)\right]^j \left[k\,\mathrm{sn}\left(\bar{\Theta} - \frac{\omega_2}{2}\right)\mathrm{sn}\left(\bar{\Theta} - \frac{5\omega_2}{6}\right)\right]^i, \tag{2.9}$$

where $\rho(\Theta - \bar{\Theta})$ is a function that we determine from the distribution of the eigenvalues and the matrix elements. Below the critical temperature Eq. (2.9) exactly gives the leading asymptotic correlation function of the triangular lattice Ising model; see Appendix A. The same may be true for general Q. Other than the correlation functions of magnetic moments, there exists a possibility to observe the minimal case (2.8) in the calculation of the anisotropic interfacial tension; we shall address this point in Sec. IV.

The analysis in Appendix A also suggests that Eq. (2.9) is naturally regarded as a candidate of correction terms to Eq. (2.8) for the triangular lattice Potts model above $T_{\mathrm{C}}(Q)$. Note that Eq. (2.9) is a higher-order term of the sn functions' pairs. The argument in this section indicates that the integral on the right-hand side of Eq. (2.8) plays the role of a building block of correlation functions.

III. NUMERICAL ANALYSES OF TRIANGULAR LATTICE Q-STATE POTTS MODEL

The Hamiltonian of the triangular lattice Q-state Potts model is given by

$$H = -J \sum_{\langle \mathbf{r}, \mathbf{r}' \rangle} [2\delta(q_{\mathbf{r}}, q_{\mathbf{r}'}) - 1] \quad (J > 0), \tag{3.1}$$

where the Q-valued variable $q_{\mathbf{r}} = 0, 1, \ldots, Q - 1$ is associated with a site in a triangular lattice $\mathbf{r} \in \Lambda_{\mathrm{tri}}$ and the sum

runs over all nearest-neighbor pairs of sites. For each $q_{\mathbf{r}}$, we introduce a spin variable $\sigma_{\mathbf{r}} = \exp(2\pi i q_{\mathbf{r}}/Q)$.

The phase transition is continuous for $Q \leqslant 4$ and first order for $Q > 4$ [13,31]. The transition temperature $T_{\mathrm{C}}(Q)$ is given by

$$\sqrt{Q}x_{\mathrm{C}}^3 + 3x_{\mathrm{C}}^2 = 1, \quad \sqrt{Q}x_{\mathrm{C}} = e^{2J/k_{\mathrm{B}}T_{\mathrm{C}}(Q)} - 1. \tag{3.2}$$

This section restricts ourselves to the disordered phase: $T > T_{\mathrm{C}}(Q)$. The spin correlation function $c(\mathbf{r})$ is defined as

$$c(\mathbf{r}-\mathbf{r}') = \langle \sigma_{\mathbf{r}}\sigma_{\mathbf{r}'}^{*}\rangle = \left\langle \exp\left[\frac{2\pi i(q_{\mathbf{r}} - q_{\mathbf{r}'})}{Q}\right]\right\rangle. \tag{3.3}$$

Some MC algorithms are known to simulate Potts models efficiently [54–56]. In the previous study of the square lattice, Q-state Potts model [28], we used a cluster MC algorithm for infinite-size systems proposed by Evertz and von der Linden [57]. It allows us to simulate off-critical systems in the thermodynamic limit directly. We can also benefit from these strong points in the numerical analysis of Eq. (3.1), which provides solid ground to check the applicability of the C_{6v} form for asymptotic correlation functions.

First, we summarize the methodological aspect of MC simulations by borrowing some notation and definitions provided in Ref. [28]. The MC algorithm is based on the Fortuin–Kasteleyn representation of the partition function of Eq. (3.1), say $Z(Q)$ [58]. Suppose $n_{\mathbf{r}^*}$ $(= 0, 1)$ is an occupation number of a site $\mathbf{r}^*$ in the medial lattice of Λ_{tri}. Then $Z(Q)$ represents a bond percolation on Λ_{tri} with the percolation probability $p(T) = 1 - e^{-\frac{J}{k_{\mathrm{B}}T}}$. Each cluster generated in the percolation process randomly possesses a Q-valued color property. Therefore, the $Q \to 1$ limit of the Potts model provides the standard bond percolation defined on Λ_{tri}.

The infinite-system MC method [57] is based on Wolff's single-cluster algorithm [56]. It fixes the seed site to the origin of a lattice $\mathbf{o}$ throughout a simulation. For disordered systems with correlation length ξ, we start with random spin configurations on finite lattice systems with linear dimension l_{B}. The initial MC steps equilibrate spin configurations within a circular domain that gradually broadens toward its outer region. We denote the ratios of an equilibrated circular domain as l_{T}, and the number of MC steps required increases exponentially as $\exp(al_{\mathrm{T}}/\xi)$. Typically, we prepare equilibrated spin configurations with $l_{\mathrm{T}} \simeq 20\xi$ and then calculate the MC averages of the correlation functions within the circular domains. We use finite systems that satisfy the condition $l_{\mathrm{B}} \gg l_{\mathrm{T}}$ (in a typical case $l_{\mathrm{B}} \simeq 4l_{\mathrm{T}}$). Then, the probability of the generated clusters touching the lattice boundary is negligible during viable MC simulation steps.

Because of the random cluster representation of the Potts model, the so-called improved estimator for the correlation functions is available: Suppose $\mathcal{C} \subset \Lambda_{\mathrm{tri}}$ is a set of sites that form a cluster. Then we evaluate the spin correlation functions as

$$c(\mathbf{r}-\mathbf{r}') = \left\langle \frac{Q\delta(q_{\mathbf{r}}, q_{\mathbf{r}'}) - 1}{Q-1}\right\rangle = \left\langle \frac{1}{|\mathcal{C}|}\delta(\mathbf{r}, \mathbf{r}'|\mathcal{C})\right\rangle_{\mathrm{MC}}, \tag{3.4}$$

where $|\mathcal{C}|$ is the number of sites in $\mathcal{C}$, and $\delta(\mathbf{r}, \mathbf{r}'|\mathcal{C}) = 1$ if $\mathbf{r}, \mathbf{r}' \in \mathcal{C}$, and $\delta(\mathbf{r}, \mathbf{r}'|\mathcal{C}) = 0$ otherwise. For $Q = 1, 2, 3$, and 4 and at several reduced temperatures $t = [T - T_{\mathrm{C}}(Q)]/T_{\mathrm{C}}(Q)$, we prepare the correlation function data and associated statistical errors as functions of $\mathbf{r} = j\mathbf{a}_1 + i\mathbf{a}_2$, say $\{c(i, j), d(i, j)\}$. In this step, we typically generate about 6×10^{15} clusters for each average calculation to satisfy a high statistical accuracy requirement (see below).

Now we check the applicability of Eq. (2.8) for the triangular lattice Q-state Potts model. For convenience, we replace ω_1 and ω_2 with I and iI', respectively. Then, the form for C_{6v} is given by

$$\begin{aligned}\mathcal{F}_{\mathrm{tri}}(i, j; A, k) = \frac{A(1-k^2)^{\frac{1}{4}}}{\pi}\int_{-I}^{I} d\varphi \\ \times \left[k\,\mathrm{sn}\left(\varphi + \frac{iI'}{6}\right)\mathrm{sn}\left(\varphi - \frac{iI'}{6}\right)\right]^{j} \\ \times \left[k\,\mathrm{sn}\left(\varphi - \frac{iI'}{2}\right)\mathrm{sn}\left(\varphi - \frac{5iI'}{6}\right)\right]^{i}.\end{aligned} \tag{3.5}$$

We represent the normalization factor using a parameter A [28], which refers to the exact value $A = 1$ for $Q = 2$; see Eq. (A11). We use the reduced χ-square statistic to fit the calculation of the C_{6v} form (3.5) for MC data and then extract optimal values by minimizing $\chi^2_{\mathrm{tri}}(A, k)$ concerning A and k:

$$\chi^2_{\mathrm{tri}}(A, k) = \sum_{(i,j)\in\mathcal{D}}\left[\frac{\mathcal{F}_{\mathrm{tri}}(i, j; A, k) - c(i, j)}{d(i, j)}\right]^2. \tag{3.6}$$

In this process, we should pay attention to a region $\mathcal{D}$ in which the form will fit the MC data. There are two types of sources of errors in fitting calculations: statistical and systematic. Equation (3.5) does not take the contributions of eigenvalues with $(\nu, \nu') \neq (2, 4)$ into account (see Appendix A), which causes a systematic error for short-distance fittings. By contrast, the longer the distances, the larger the statistical error of MC data, which causes uncertainty in the estimated optimal values. As discussed in Ref. [28], to control the two types of errors, we use an annular region defined as $\mathcal{D}(c_{\max}, c_{\min}) = \{(i, j)|c_{\min} < c(i, j) < c_{\max}\}$ and check the $\mathcal{D}$ dependence of the fitting conditions.

We determine a lower cutoff $c_{\min}$ so that a statistical error does not affect the fitting. As mentioned above, we perform large-scale MC calculations, which allow us to use a small value independently of Q, for example, $c_{\min} = 10^{-7}$. We should determine the upper cutoff $c_{\max}$ according to the magnitude of systematic errors. For $Q = 2$, the correction from the second-band eigenvalues is absent because of $\mathbb{Z}_2$ symmetry; see Appendix A and Ref. [28]. However, for $Q \neq 2$, it does exist in the MC data. Therefore, we use $c_{\max}$ depending on Q; see below.

Once we obtain the optimal values, say $\bar{A}$ and $\bar{k}$, the correlation function is asymptotically given by $c(\mathbf{r}) \sim \bar{\mathcal{F}}_{\mathrm{tri}}(i, j) = \mathcal{F}_{\mathrm{tri}}(i, j; \bar{A}, \bar{k})$. From this expression, we can find the ACLs for the Q-state Potts model; see Sec. IV A.

A. Potts model with $Q = 2$

First, we analyze the triangular lattice Ising model because the exact results are available to check our numerical procedure's accuracy. The second part of Table III summarizes the fitting results. The geometrical properties of $\mathcal{D}$ and the ACLs in the row and diagonal directions are given for several

TABLE III. Temperature dependence of the optimal values and ACLs in the row and diagonal directions. Annular domains $\mathcal{D}(C_{\max}, 10^{-7})$ with $C_{\max} = 10^{-4}$, 10^{-2}, 10^{-4}, and 5×10^{-5} were used for $Q = 1, 2, 3$, and 4, respectively. Underlined digits in the second part coincide with the exact values and parenthesized numbers are error estimates.

Q	t	$\lvert\mathcal{D}\rvert$	$\bar{k}$	$\bar{A}$	ξ_{row}	ξ_{diag}
1	0.50	3462	0.6414103(7)	1.0331304(205)	3.0054826(63)	3.0054714(63)
	0.65	2076	0.5615632(8)	1.0261963(185)	2.3146357(57)	2.3146114(57)
	1.00	966	0.4245572(4)	1.0166832(89)	1.5621318(17)	1.5620547(17)
	1.50	510	0.3036457(1)	1.0100107(5)	1.1265246(3)	1.1263275(3)
	2.00	336	0.2299296(5)	1.0066811(124)	0.9164885(13)	0.9161383(13)
	5.00	108	0.0792507(11)	1.0021472(566)	0.5402944(30)	0.5389299(31)
	14.00	66	0.0195738(5)	0.9999633(50)	0.3571421(2)	0.3538792(2)
2	0.20	5994	0.6800375(4)	1.0000052(55)	3.4604115(52)	3.4604041(52)
	0.30	3042	0.5789032(6)	1.0000020(83)	2.4429856(46)	2.4429648(46)
	0.50	1344	0.4385518(7)	1.0000037(57)	1.6231582(18)	1.6230892(18)
	1.00	522	0.2588192(3)	0.9999989(43)	0.9952521(8)	0.9949732(8)
	2.00	234	0.1290396(4)	0.9999965(64)	0.6635029(9)	0.6626786(9)
	5.00	114	0.0421156(0)	1.0000003(1)	0.4373675(0)	0.4351778(0)
	10.00	66	0.0164018(0)	0.9999957(78)	0.3428788(5)	0.3393696(5)
3	0.15	2490	0.6267329(4)	0.9615277(102)	2.8568853(19)	2.8568723(19)
	0.20	2046	0.5597793(4)	0.9679882(105)	2.3019859(28)	2.3019611(28)
	0.30	1164	0.4590180(0)	0.9765406(10)	1.7176157(0)	1.7175572(0)
	0.50	582	0.3320364(4)	0.9856334(119)	1.2166812(13)	1.2165227(13)
	1.00	258	0.1859817(8)	0.9938120(222)	0.8032343(20)	0.8027337(20)
	2.00	144	0.0896159(2)	0.9974591(132)	0.5666246(5)	0.5654062(5)
	8.00	42	0.0151040(3)	1.0002672(340)	0.3366384(12)	0.3330153(13)
4	0.10	2874	0.6265930(2)	0.9176194(7)	2.8555249(19)	2.8555119(19)
	0.14	1812	0.5552042(22)	0.9321563(549)	2.2699906(152)	2.2699648(152)
	0.20	1152	0.4739819(12)	0.9468457(269)	1.7909835(60)	1.7909317(60)
	0.30	684	0.3793838(12)	0.9619715(266)	1.3821942(45)	1.3820842(45)
	0.50	384	0.2667541(14)	0.9776521(388)	1.0176226(40)	1.0173604(40)
	1.00	186	0.1449223(5)	0.9915611(105)	0.7020979(12)	0.7013848(12)
	2.00	108	0.0685188(9)	0.9956911(506)	0.5122705(24)	0.5107258(24)
	6.00	42	0.0168894(3)	0.9984632(330)	0.3451569(12)	0.3416882(12)

reduced temperatures t, where $|\mathcal{D}|$ denotes the number of sites in $\mathcal{D}$. Concerning $c_{\max}$, we observe that the fitting condition is almost independent of it, and thus use a larger value, that is, $c_{\max} = 10^{-2}$, to improve statistical accuracy.

Then we find that the optimized parameters agree well with the exact values, that is, at all temperatures, they yield $\bar{A} = A_{\text{exact}} = 1$ and $\bar{k} = k_{\text{exact}}$ with at least six-digit accuracy. In the table, note that the underlined digits coincide with the exact values and the parenthesized digits are error estimates. As t decreases, the directional dependence of the correlation length becomes weaker; hence, highly accurate numerical data are necessary for its detection. The second part of Table III shows that our numerical approach using the form (3.5) is sufficiently efficient to analyze the ACLs with C_{6v} symmetry (see ξ_{row} and ξ_{diag}).

In our previous paper [28], we proposed the C_{4v} form and established its goodness of fit for correlation functions of the square lattice Potts model. Naturally, we expect that the advantages explained contribute to the present high accuracy. Additionally, as given in Sec. II, C_{6v} symmetry reduces the number of free parameters in the form to two. Therefore, we recognize that the triangular lattice offers a more suitable framework for studying the directional dependence of correlation functions.

B. Potts model with $Q \neq 2$

Next, we investigate the applicability of Eq. (3.5) to the $Q = 1$, 3, and 4 Potts model. In the C_{4v} case, the deformation parameter, b (=1 for the Ising case), exists and represents the Q dependence of the ACLs; see Sec. III of Ref. [28]. By contrast, Eq. (3.5) only includes amplitude A and modulus k (see Secs. II and IV). If the form can fit the correlation function data independently of Q, then it provides strong numerical evidence for the wide applicability of Eq. (3.5), including unsolvable cases. Simultaneously, it leads us to the conjecture that triangular lattice models that satisfy the three conditions in Sec. II can exhibit a unique ACL identical to the Ising model.

Because the fittings suffer from corrections that originate from the second band of eigenvalues, annuli with a larger cutoff $c_{\max}$ than the Ising case should be used [28]. Following the same procedure as the Ising case, we optimize the cutoff as $c_{\max} = 10^{-4}$, 10^{-4}, and 5×10^{-5} for $Q = 1$, 3, and 4, respectively; a finer optimization may be possible by taking temperature dependence into account, but we avoided it for clarity.

We summarize the results in Table III. Compared with the Ising case, the fitting conditions worsen because the correlation function data include larger errors in outer regions.

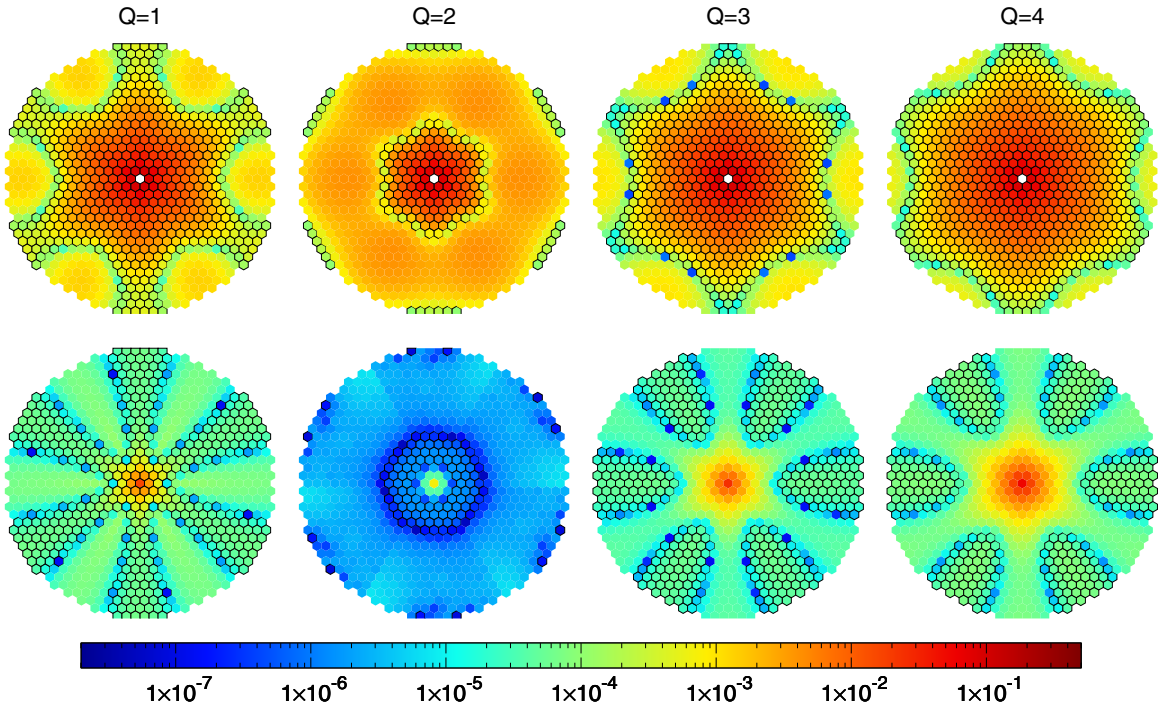

FIG. 3. The first and second rows show the color maps of the residual errors $\mathcal{R}_{\rm OZ}(i,\,j)$ and $\mathcal{R}_{\rm tri}(i,\,j)$, respectively. From left to right, their comparisons are given for $Q = 1$, 2, 3, and 4 at $t = 1$, 0.5, 0.3, and 0.2, respectively. Each site $(i,\,j)$ corresponds to one hexagon whose color represents $|\mathcal{R}_{\rm OZ}|$ or $|\mathcal{R}_{\rm tri}|$. Boundary lines of hexagons indicate that the residual errors are positive.

Additionally, the decrease of $|\mathcal{D}|$ may cause a lowering of the statistical accuracy of the estimates of optimal values. Despite this, we find that our procedure estimates $\bar{A}$ and $\bar{k}$ within four or five-digit accuracy based on the following observations: First, deep in the disordered phase, we theoretically expect the amplitude to be $A \simeq 1$. The estimates $\bar{A}$ in the table agree with this condition and converge to 1 for large t independently of Q. Second, in the second row of Fig. 3, we provide color maps of reduced residual errors in fittings between $\bar{\mathcal{F}}_{\rm tri}(i,\,j)$ and $c(i,\,j)$ defined by

$$\mathcal{R}_{\rm tri}(i,\,j) = \frac{\bar{\mathcal{F}}_{\rm tri}(i,\,j) - c(i,\,j)}{c(i,\,j)}. \tag{3.7}$$

One hexagon corresponds to each site $(i,\,j)$, whose color represents the absolute value $|\mathcal{R}_{\rm tri}|$ and whose boundary line represents its sign, that is, we draw boundary lines for hexagons if the residual errors are positive. We see that the optimized form asymptotically fits the MC data in all directions, excluding the central circular domain. Compared with the $Q = 2$ case, the directional dependence of residuals is visible for $Q \neq 2$, which can be attributed to the second-band eigenvalue corrections; see Sec. II B. As a result, we confirm that the form (3.5) can also fit unsolvable models' asymptotic correlation functions, although their accuracy is lower by about 1 or 2 digits than that in the Ising case.

C. Comparison with the Ornstein–Zernike form

Following the square lattice case [28], we have provided a second example in which the form extracted from the three conditions (i)–(iii) combined with the lattice symmetry (see Sec. II) well describes the asymptotic behavior of correlation functions. Indeed, we observed that Eq. (3.5) could fit the correlation functions of the triangular lattice Q-state Potts model and clarified its wide applicability.

Now we compare fitting qualities between the present form and OZ form: $\mathcal{F}_{\rm OZ}(i,\,j;B,\,\xi) = Be^{-R/\xi}/\sqrt{R}$ $(R \neq 0)$. $\mathcal{F}_{\rm OZ}$ has been widely used to analyze the correlation functions in disordered phases. Note that Eqs. (2.1), (2.7), (2.8), and (3.5) yield the OZ form by the saddle point method, and thus our form is compatible with the OZ form for larger distances.

To clarify the difference in degree consistent with MC data, we perform the same fitting calculations using $\chi^2_{\rm OZ}(B,\,\xi)$ statistics, that is, we replace the measure $\mathcal{F}_{\rm tri}$ in Eq. (3.6) with $\mathcal{F}_{\rm OZ}$, but keep the annular regions $\mathcal{D}$ the same in both cases. We denote the optimized value by $\bar{B}$ and $\bar{\xi}$, and define the reduced residual errors of fittings as $\mathcal{R}_{\rm OZ}(i,\,j) = [\bar{\mathcal{F}}_{\rm OZ}(i,\,j) - c(i,\,j)]/c(i,\,j)$, where $\bar{\mathcal{F}}_{\rm OZ}(i,\,j) = \mathcal{F}_{\rm OZ}(i,\,j;\bar{B},\,\bar{\xi})$. The color maps of the residuals are displayed in the first row of Fig. 3.

Although the number of free parameters is the same, the quality of fitting using the OZ form is much lower than that using the form (1.5). This discrepancy indicates the existence of large systematic errors in the OZ form and identifies its insufficiency in describing the off-critical correlation functions. As the comparison in the $Q = 2$ case demonstrates, although $\mathcal{R}_{\rm tri}$ is seemingly rotational symmetric, $\mathcal{R}_{\rm OZ}$ is C_{6v} symmetric in direction, which reflects the lack of discrete properties in the OZ form. Similarly, comparing other cases demonstrates the advantage of the present C_{6v} form. One might expect that the OZ form can improve its fitting quality by introducing an anisotropic correlation length, i.e., $\xi(\theta)$. In principle, this may be correct, but in the reality of fitting calculations to MC data,

the larger errors in the estimates due to the increase of degrees of fitting parameters and statistical errors are inevitable; see Appendix B in Ref. [28].

Meanwhile, $\mathcal{R}_{\rm tri}$ clearly shows an oscillation accompanied by the sign changes in the angular direction. Intriguingly, $\mathcal{R}_{\rm tri} < 0$ and $\mathcal{R}_{\rm tri} > 0$ in the row and diagonal directions, respectively for $Q = 1$, whereas they take the opposite sign for $Q = 3$ and 4. Because the correction from the second-band eigenvalues mainly contributes to the residual errors, its sign for $Q < 2$ is seemingly the opposite of that for $Q > 2$. Indeed, this prediction is consistent with the exact result (and the numerical result) that the correction from the second-band eigenvalues Eq. (2.9) vanishes for $Q = 2$. As a result, the observed Q-dependent pattern in Fig. 3 implies a possibility of canonically improving the leading form $\mathcal{F}_{\rm tri}$ by taking correction terms into account; see also Sec. IV.

IV. DISCUSSION AND SUMMARY

We investigated the leading asymptotic behavior of the correlation functions of the Q-state Potts model on a triangular lattice. In Sec. II, following the argument for C_{4v} [28,53], we constructed asymptotic forms for C_{6v}. First, we took the three properties (i)–(iii) into account, which are expected to be connected with C_{2v} symmetry directly. Our exact analyses in Appendix A showed that the asymptotic correlation function of the triangular lattice Ising model satisfies (i)–(iii). We assumed that the three properties are widely applicable to the models on the triangular lattice, whether solvable or not. Then, we found that the asymptotic correlation function is written as integrals of the products of sn functions. Based on this integral representation, we derived the asymptotic form for C_{6v} using the fact that C_{2v} is the normal subgroup of C_{6v}. The product structure of the sn functions is essentially the same as that of C_{4v} [28]. By contrast, unlike the C_{4v} case, where the fitting forms include three or more free parameters, we found the minimal case, which has only two parameters: the normalization constant A and modulus k.

From the exact analyses for $Q = 2$, we indicated that the minimal form (2.8) [or (3.5)] applies to the general-Q Potts model above transition temperatures. We performed MC simulations using the infinite-size algorithm [57] for $Q = 1,\ 2,\ 3,\ 4$ above $T_{\rm C}(Q)$ and then successfully fit the MC data with about five-digit accuracy. It is worth noting that, although there were fewer free parameters, we performed the fittings with the same accuracy as the square lattice model calculations [28]. The present observation indicates the validity of the minimal form for correlation functions and the efficiency of using our approach to study triangular lattice models.

In Ref. [28] and this paper, we applied the three properties (i)–(iii) to massive dispersion curves. Although we cannot prove them rigorously, these are expected to be reasonable working hypotheses. Using them, we derived a possibility of systematic deformations for general Q from the exact result Eq. (1.1) in the C_{4v} case, and the Q-independent minimal form (2.8) here. These were confirmed numerically in quite high accuracy. We expect the argument in Sec. II based on point groups is applicable to a wide class of lattice models; see also the argument in Sec. II of Ref. [28]. Finding the minimal form is the main result in this paper. The minimal form with two parameters indicates the existence of an algebraic curve containing one parameter. We can point out a possibility that this algebraic curve plays the important role as a temperature scale. In the following, we discuss the ECS [1,4] to clarify the physical meaning of the minimal form. We show that the ECS derived from the ACL is given by a simple algebraic curve of genus 1. Furthermore, the product structures of sn functions relate to differential forms on the algebraic curve. Using birational transformations, we indicate an important role of modulus k in representing the weak universality concept [59] in critical phenomena.

A. Equilibrium crystal shape for the honeycomb lattice

In this subsection, we derive the ECS for the honeycomb lattice from the asymptotic correlation function in Sec. III. Suppose that i and j become large with i/j fixed to be a constant in Eq. (3.5). We introduce angle θ between the directions of $\mathbf{a}_1$ and $j\mathbf{a}_1 + i\mathbf{a}_2$ as follows:

$$R\cos\theta = j - \frac{1}{2}i, \quad R\sin\theta = \frac{\sqrt{3}}{2}i \ \text{ with } R = \sqrt{j^2 + i^2 - ij} \tag{4.1}$$

(see Fig. 1). We estimate the integral on the right-hand side using the method of steepest descent. We calculate ACL ξ as follows:

$$-\frac{1}{\xi} = \frac{2}{\sqrt{3}}\left\{ \cos\left(\theta - \frac{\pi}{6}\right) \ln\left[k\,\mathrm{sn}\left(\phi_{\rm s} + \frac{iI'}{6}\right)\mathrm{sn}\left(\phi_{\rm s} - \frac{iI'}{6}\right)\right] + \sin\theta \ln\left[k\,\mathrm{sn}\left(\phi_{\rm s} - \frac{iI'}{2}\right)\mathrm{sn}\left(\phi_{\rm s} - \frac{5iI'}{6}\right)\right]\right\}, \tag{4.2}$$

where we determine the saddle point $\phi_{\rm s}$ as a function of θ by

$$\cos\left(\theta - \frac{\pi}{6}\right)\mathrm{sn}(2\phi_{\rm s})\sinh\left\{\ln\left[k\,\mathrm{sn}\left(\phi_{\rm s} + \frac{iI'}{6}\right)\mathrm{sn}\left(\phi_{\rm s} - \frac{iI'}{6}\right)\right]\right\} + \sin\theta\,\mathrm{sn}\left(2\phi_{\rm s} - \frac{4iI'}{3}\right)\sinh\left\{\ln\left[k\,\mathrm{sn}\left(\phi_{\rm s} - \frac{iI'}{2}\right) \times \mathrm{sn}\left(\phi_{\rm s} - \frac{5iI'}{6}\right)\right]\right\} = 0, \tag{4.3}$$

with the condition $\phi_{\rm s} = I$ for $\theta = 0$. Then, the duality [51] relates ξ on the triangular lattice to the anisotropic interfacial tension $\gamma_{\rm h}^*$ below the transition temperature on the honeycomb lattice as follows:

$$\frac{\gamma_{\rm h}^*}{k_{\rm B}T_{\rm h}^*} = \frac{1}{\xi} \ \text{ in all directions} \tag{4.4}$$

(also see Refs. [26] and [49]). The reduced interaction constant on the honeycomb lattice $J_{\rm h}/k_{\rm B}T_{\rm h}^*$ is given by

$$\mathrm{e}^{2J_{\rm h}/k_{\rm B}T_{\rm h}^*} - 1 = \frac{Q}{\mathrm{e}^{2J/k_{\rm B}T} - 1}. \tag{4.5}$$

From $\gamma_{\rm h}^*$, we can determine the ECS for the honeycomb lattice using Wulff's construction: We denote the point on the ECS by (X, Y), use Eq. (4.2) in Ref. [28] with $\theta_\perp$ replaced by θ, and define the exponentials as follows:

$$\alpha = \exp(-\Lambda X), \quad \beta = \exp\left[-\Lambda\left(\frac{\sqrt{3}Y}{2} - \frac{X}{2}\right)\right], \tag{4.6}$$

where Λ is a scale factor used to adjust an area of the ECS. Then, the ECS is given by

$$\alpha = k\mathrm{sn}\left(\phi + \frac{iI'}{6}\right)\mathrm{sn}\left(\phi - \frac{iI'}{6}\right),$$
$$\beta = k\mathrm{sn}\left(\phi - \frac{iI'}{2}\right)\mathrm{sn}\left(\phi - \frac{5iI'}{6}\right). \tag{4.7}$$

As ϕ moves from I to $I + 2iI'$ on the line $\Re(\phi) = I$, for example, (X, Y) sweeps out the ECS; see Fig. 5 in Ref. [49] or Fig. 6(a) in Ref. [60]. Generally, the ECSs are written in a compact form [25]. In the present case, we can rewrite Eq. (4.7) as

$$\alpha^2\beta^2 + 1 + (\alpha\beta + 1)(\alpha + \beta) + H\alpha\beta = 0, \tag{4.8}$$

with

$$H = 2\frac{\mathrm{dn}^3\left(\frac{2iI'}{3}\right) + 1}{k^2\mathrm{sn}^2\left(\frac{2iI'}{3}\right)}. \tag{4.9}$$

B. Birational transformations among algebraic curves

Equation (4.8) defines an algebraic curve on the $\alpha\beta$ plane. By introducing the homogeneous coordinate, we find two nodes at its infinity [52,61]. According to the so-called genus formula in Chap. 2.1 of Ref. [61], Eq. (4.8) is an algebraic curve of genus 1. With this in mind, we return to the correlation functions in the minimal case. Using Eq. (4.8), we can re-express Eq. (3.5) as

$$\mathcal{F}_{\mathrm{tri}}(i, j; A, k) = A\oint d\alpha \oint d\beta \frac{\alpha^j\beta^i}{\alpha^2\beta^2 + 1 + (\alpha\beta + 1)(\alpha + \beta) + H\alpha\beta}, \tag{4.10}$$

where the contour integrals are performed along the unit circles on the complex planes [16,25,26,46]. This expression shows that the product structure of sn functions in Eq. (2.8) can be regarded as polynomials on the algebraic curve (4.8) on the $\alpha\beta$ plane.

The same expression was also obtained for the Ising models on the honeycomb, diced, and Kagomé lattices in Ref. [26]; thus Eq. (4.10) is a universal leading asymptotic form with C_{6v}. As mentioned in Appendix A 2, unlike in C_{4v} case, solvable models with C_{6v} do not necessarily have structures of commuting transfer matrices. We have numerically demonstrated that the product structure on the algebraic curve (4.8) deduced from the C_{6v} symmetry describes leading asymptotic correlation functions of triangular lattice models, including unsolvable ones. As a common correction term for general Q, we derived Eq. (2.9). Meanwhile, the second row of Fig. 3 showed Q-dependent corrections, which implies a possibility that different forms exist from Eq. (4.8) for $Q \neq 2$. In most of the solvable lattice models, the asymptotic behavior of the correlation functions is rather simple since so-called bound states are absent (see, for example, the expansion in Ref. [46]); a well-known exception is the eight-vertex model [13]. It is important to examine whether the Q-dependent correction is explainable by Eq. (2.9) or not. We will address this point in future research.

As we considered the bond percolation, i.e., the $Q \to 1$ limit, in Sec. III B to find that Eq. (3.5) applies to it, lattice models without transfer matrices attract attention. For example, while the Q-state Potts model possesses discrete variables, the XY model [62,63] is defined by continuous variables. Its numerical study is currently in progress. Further investigation from the viewpoint of symmetry is also needed: Since C_{6v} contains C_{3v} as a normal subgroup as well as C_{2v}, the Ising model on the honeycomb lattice and the hard-hexagon model are worth investigating. As mentioned in Sec. II, for $T < T_{\mathrm{C}}(Q)$, we expect that the form in the next to the minimal case (2.9) gives the leading asymptotic behavior of the correlation function. According to the analysis in Sec. IV A, to find the minimal case, we should consider the anisotropic interfacial tension that is related to the ACL of the honeycomb lattice Potts model in the disordered phase. Thus, a numerical study of the honeycomb lattice Potts model is important (in this respect, note that the minimal case was found in the antiferroelectric ordered regime of the Kagomé lattice eight-vertex model [50]). We will report on this point next publication.

At the beginning of this section, we argued the wide applicability of our method based on both the three properties (i)–(iii) and the lattice symmetries. However, as mentioned in Sec. IV B of Ref. [28], the modified KDP model is an exceptional example because it does not satisfy (i)–(iii) [26,64]. In general, our method applies not to all but to a certain range of lattice models. To consider its applicability, one important clue is the birational equivalence concept. The algebraic curves here and in Ref. [28] are related to each other by birational transformations, but the algebraic curve for the modified KDP model is not.

Lastly, based on the birational equivalence, we discuss that the algebraic curve (4.8) plays a role of a universal scale to measure an amount of deviation from criticalities. As observed, it is common among models with C_{6v} symmetry and contains only one parameter H, or equivalently, k by which we determine H via Eq. (4.9). Additionally, it is independent of the types of criticalities. Hence, the shapes of the algebraic curve can specify the deviations from criticalities. Meanwhile, this argument is restricted to models with C_{6v} symmetry. We can extend it to include a wider class of models with different lattice symmetries, for example, C_{2v} and C_{4v}. As mentioned in Ref. [28], in performing this extension, birational equivalence among algebraic curves plays a crucial role. We demonstrate such an extension by considering C_{4v} symmetry as an example.

We obtained the asymptotic form for the square lattice Q-state Potts model, that is, $\mathcal{F}_{\mathrm{sq}}(i, j; A, k, b)$ [28]. We denote the point on the ECS by (X', Y'), and write the exponentials as

$$\alpha' = \exp(-\Lambda X'), \quad \beta' = \exp(-\Lambda Y'). \tag{4.11}$$

We find that they satisfy Eq. (1.2), that is,

$$\alpha'^2\beta'^2 + 1 + \bar{A}_2(\alpha'\beta' + 1)(\alpha' + \beta') + \alpha'^2 + \beta'^2 + \bar{A}_4\alpha'\beta' = 0. \tag{4.12}$$

This is also an algebraic curve of genus 1. If the values of k in Eqs. (4.8) and (4.12) are the same, then we can suitably choose rational functions to connect the variables of these two

curves:

$$\alpha' = \frac{\alpha + c}{1 + c\alpha}, \quad \beta' = \frac{\Phi_1(\alpha, \beta)}{\Phi_2(\alpha, \beta)}, \tag{4.13}$$

with

$$c = -k\mathrm{sn}\left(b\frac{iI'}{4} + \frac{iI'}{6}\right)\mathrm{sn}\left(b\frac{iI'}{4} - \frac{iI'}{6}\right), \tag{4.14}$$

where $\Phi_1(\alpha, \beta)$ and $\Phi_2(\alpha, \beta)$ are the polynomials of α, β. Because a lengthy calculation is required, we provide the details of their derivation in Appendix B. Additionally, we find the inverse transformation from α', β' to α, β; hence, the transformation is bidirectional.

To understand the implications of the transformation, we consider the critical limit by taking $k \to 1$. Using the conjugate modulus transformation, from Eq. (4.13), we obtain a transformation between the ECS in Sec. IV A and that in Sec. IV of Ref. [28]. It follows that

$$k \sim 1 - 8q', \quad q' = \exp\left(-\pi\frac{I}{I'}\right). \tag{4.15}$$

Note that the conjugate nome $q' \sim 1/\xi$. To fix the areas of the ECSs, we adjust the scale factor as follows:

$$\Lambda = q'. \tag{4.16}$$

Then, Eqs. (4.6) and (4.11) reduce to

$$\alpha \sim 1 - \Lambda X, \quad \beta \sim 1 - \Lambda\left(\frac{\sqrt{3}Y}{2} - \frac{X}{2}\right) \tag{4.17}$$

and

$$\alpha' \sim 1 - \Lambda X', \quad \beta' \sim 1 - \Lambda Y', \tag{4.18}$$

respectively. Equations (4.8) and (4.12) show that the ECSs become circles near the critical point; only their radii are different. From the transformation (4.13), we find that

$$\sqrt{X'^2 + Y'^2} = \frac{\cos\frac{b\pi}{4}}{\cos\frac{\pi}{6}}\sqrt{X^2 + Y^2}. \tag{4.19}$$

To explain the continuously varying exponents in the eight-vertex model [13,43], Suzuki proposed the weak universality concept [59], where the inverse correlation length $1/\xi$ was regarded as a natural scale to measure the departure from critical points. The relation (4.19) indicates that to match the correlation length given in Sec. IV A with that in Ref. [28], dilatation by the amount of $\cos(b\pi/4)/\cos(\pi/6)$ is required, which depends on both the degrees of freedom (like Q) and the types of lattices (e.g., triangle and square). In this respect, birational equivalence states that k is more fundamental than $1/\xi$.

Because the birational transformation (4.13) is well-defined for general k, including the $k \to 1$ limit, the modulus can provide a universal measure of the departure from critical points among various models defined on different lattices. Mathematically, birational equivalence is a basic concept in the field of algebraic geometry [52]. In addition to the genus, k is known as a birational invariant. It is strongly suggested that the rich structures of birational geometry introduce a new insight into the study of lattice models.

ACKNOWLEDGMENTS

We thank Professors Macoto Kikuchi, Yasuhiro Akutsu, and Yutaka Okabe for stimulating discussions. The main computations were performed using the facilities at Tohoku University and Tokyo Metropolitan University. This research was supported by JSPS KAKENHI Grant No. 26400399.

APPENDIX A: ASYMPTOTIC CORRELATION FUNCTIONS FOR $Q = 2$

In Appendix A of Ref. [28], we investigated the correlation length in the square lattice Ising model by extending the method of commuting transfer matrices in Chap. 7 of Ref. [13] using the shift operator. In this Appendix, we apply the same method to the Ising model on the triangular lattice. We define inhomogeneous systems on the square lattice. Each system still possesses a one-parameter family of commuting transfer matrices. The products of commuting transfer matrices yield transfer matrices on the triangular lattice. We analyze the asymptotic correlation function along 12 directions and then find the three properties (i)–(iii) in Ref. [28] that hold for the triangular lattice. This result supports our discussion on obtaining the asymptotic correlation functions with C_{6v} symmetry in Sec. II.

1. Inhomogeneous transfer matrices

First, we draw a square lattice diagonally. For the Ising model, each $\sigma_{\mathbf{r}}$ takes the values of ± 1 because it is defined as $\sigma_{\mathbf{r}} = \exp(i\pi q_{\mathbf{r}})$ with $q_{\mathbf{r}} = 0, 1$ (see Sec. III). The Hamiltonian is written as Eq. (A1) in Ref. [28], where the nearest-neighbor spins are coupled by J or J' depending on the direction. Using Jacobi's elliptic functions, we parametrize the reduced coupling constants $K = J/k_{\mathrm{B}}T$, $K' = J'/k_{\mathrm{B}}T$ using Eq. (A5) in Ref. [28] for $T > T_{\mathrm{C}}$ and Eq. (A6) in Ref. [28] for $T < T_{\mathrm{C}}$. To investigate the triangular lattice Ising model, we suppose that the spectral parameter u varies from site to site [13]. We introduce a real number v_0 and define inhomogeneous transfer matrices. We consider two successive rows, and let $\sigma = \{\sigma_0, \ldots, \sigma_{N-1}\}$ and $\sigma' = \{\sigma'_0, \ldots, \sigma'_{N-1}\}$ be two sets of spins in the lower and upper rows, respectively (N even); see Fig. 4. We assume periodic boundary conditions in both

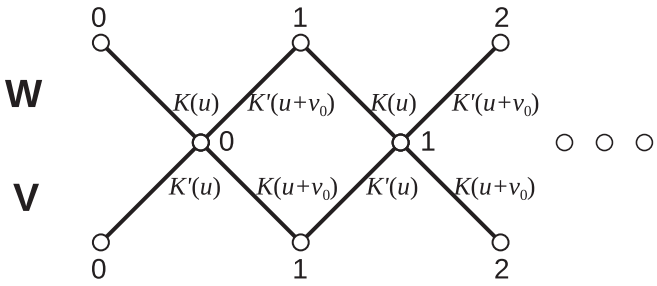

FIG. 4. Square lattice is drawn diagonally. Transfer matrices **W** and **V** connect three successive rows. For the parametrization of coupling constants, see the text.

directions. Then, the transfer matrices $\mathbf{V}$ and $\mathbf{W}$ are given by elements as follows:

$$[\mathbf{V}(u)]_{\sigma,\sigma'} = \exp\left\{\sum_{l=0}^{N-1}[K'(u)\sigma_l\sigma_l' + K(u+v_0)\sigma_{l+1}\sigma_l']\right\},$$
$$[\mathbf{W}(u)]_{\sigma,\sigma'} = \exp\left\{\sum_{l=0}^{N-1}[K(u)\sigma_l\sigma_l' + K'(u+v_0)\sigma_l\sigma_{l+1}']\right\}, \tag{A1}$$

where $\sigma_N = \sigma_0$ and $\sigma_N' = \sigma_0'$. We regard modulus k and v_0 as fixed constants. They satisfy the following commutation relations:

$$[\mathbf{V}(u), \mathbf{V}(u')] = [\mathbf{W}(u), \mathbf{W}(u')] = [\mathbf{V}(u), \mathbf{W}(u')] = 0 \quad \forall u,\ u' \in \mathbb{C}. \tag{A2}$$

We denote the eigenvalues of $\mathbf{V}(u)$ and $\mathbf{W}(u)$ by $V(u)$ and $W(u)$, respectively. Then, as $N \to \infty$,

$$V(u) \sim \kappa(u)^{\frac{N}{2}}\kappa(u+v_0)^{\frac{N}{2}}, \quad W(u) \sim \kappa(u)^{\frac{N}{2}}\kappa(u+v_0)^{\frac{N}{2}}, \tag{A3}$$

where $\kappa(u)$ is given by Eqs. (A14)–(A16) in Ref. [28]; also see Chap. 11 of Ref. [13]. To calculate the asymptotic correlation function, we define the following limiting functions:

$$\lim_{N\to\infty}\frac{W(u)}{[\kappa(u)\kappa(u+v_0)]^{\frac{N}{2}}}, \quad \lim_{N\to\infty}\frac{V(u)}{[\kappa(u)\kappa(u+v_0)]^{\frac{N}{2}}}. \tag{A4}$$

In Ref. [28], we proved that they are the same form and satisfy Eq. (A27) or Eq. (A28). Thus, we write both of them as

$$\pm\prod_{l=1}^{\mu} k^{\frac{1}{2}}\mathrm{sn}\left(-\phi_l + \frac{iI'}{2} + iu + \frac{iv_0}{2}\right). \tag{A5}$$

As a result, we label the limiting function using μ-real variables $\phi_1, \ldots, \phi_\mu$. We denote it by $L(\phi_1, \ldots, \phi_\mu|u)$.

To investigate the triangular lattice Ising model with the isotropic interaction, we set $v_0 = I'/3$ and take the limits of u as follows: The transfer matrix can be constructed as

$$\mathbf{Y} = \lim_{\substack{u_1\to 0\\ u_2\to 2v_0}} \mathbf{W}\left(\frac{I'}{3}\right)\frac{\mathbf{V}(u_1)}{\kappa(u_1)^{\frac{N}{2}}}\mathbf{W}\left(\frac{I'}{3}\right)\frac{\mathbf{V}(u_2)}{\kappa(u_2+v_0)^{\frac{N}{2}}}, \tag{A6}$$

and the shift operator as

$$\mathbf{X} = \lim_{\substack{u_1\to I'\\ u_2\to 2v_0}} \frac{\mathbf{W}(u_1)}{[\kappa(u_1)\kappa(u_1+v_0)]^{\frac{N}{2}}}\frac{\mathbf{V}(u_2)}{[\kappa(u_2)\kappa(u_2+v_0)]^{\frac{N}{2}}}. \tag{A7}$$

We showed in Appendix A of Ref. [28] that the asymptotic correlation function is calculated from two ratios L_Y and L_X; the former (latter) denotes the ratio between the eigenvalues and the largest eigenvalue of $\mathbf{Y}$ ($\mathbf{X}$); see also Refs. [34–36]. Using $L(\phi|u)$, they are represented as

$$L_X(\phi) = L(\phi|I')L\left(\phi\middle|\frac{2I'}{3}\right),$$
$$L_Y(\phi) = L\left(\phi\middle|\frac{I'}{3}\right)L(\phi|0)L\left(\phi\middle|\frac{I'}{3}\right)L\left(\phi\middle|\frac{2I'}{3}\right). \tag{A8}$$

In the $N \to \infty$ limit, the summation over eigenvalues becomes integrals because of their continuous distribution. In particular, for $T > T_C$, we calculate the leading asymptotic behavior of the correlation function from a band of the next-largest eigenvalues with $\mu = 1$. For $\mathbf{r} = j\mathbf{a}_1 + i\mathbf{a}_2$ (see Fig. 1), it is given by the integral with respect to ϕ_1 as

$$\langle\sigma_{\mathbf{o}}\sigma_{\mathbf{r}}\rangle \sim \int_{-I}^{I} d\phi_1\ \rho(\phi_1) \times\left[k\mathrm{sn}\left(-\phi_1 - \frac{iI'}{3}\right)\mathrm{sn}\left(-\phi_1 - \frac{2iI'}{3}\right)\right]^j \times\left[k\mathrm{sn}(-\phi_1 - iI')\mathrm{sn}\left(-\phi_1 - \frac{4iI'}{3}\right)\right]^i, \tag{A9}$$

with

$$\sinh K = \frac{i}{\mathrm{sn}\left(\frac{2iI'}{3}\right)}, \tag{A10}$$

where $\rho(\phi_1)$ is to be determined from the distribution of the eigenvalues and the matrix elements. Note that the minimal form (2.8) with $(\nu, \nu') = (2, 4)$ coincides with Eq. (A9) if we change the integration variable to $\Theta = -\phi_1 - iI'/2$ and shift the integration path suitably. Because of $\mathbb{Z}_2$ symmetry, the contribution of the next-to-next-largest eigenvalues with $\mu = 2$ vanishes. Therefore, the first correction to the asymptotic behavior (A9) originates from $\mu = 3$ (see the numerical results in Sec. III C).

When i and j become large with i/j fixed, we can calculate the correlation length ξ along the direction θ by shifting the integration path and using the method of steepest descent [43]; θ is related to i and j by $\tan\theta = \sqrt{3}\,i/(2j - i)$; see Sec. IV A. Increasing θ by 2π causes the saddle point to move by $2iI'$ on the line $\Re(\phi_1) = I$. We expect that $\rho(\phi_1)$ is a doubly periodic function and is analytic inside a periodic rectangle. According to Liouville's theorem, it should be a constant. Because the normalization constant is identical to that of the square lattice Ising model,

$$\rho(\phi_1) = \frac{(1-k^2)^{\frac{1}{4}}}{\pi} \tag{A11}$$

[65]; see also Chap. 11 of Ref. [13].

For $T < T_C$, the two largest eigenvalues are asymptotically degenerate as $N \to \infty$. The next-largest eigenvalues correspond to the case $\mu = 2$. Thus, the asymptotic correlation function is given by the double integral with respect to ϕ_1, ϕ_2 as

$$\langle\sigma_{\mathbf{o}}\sigma_{\mathbf{r}}\rangle - \langle\sigma_{\mathbf{o}}\rangle\langle\sigma_{\mathbf{r}}\rangle \sim \int_{-I}^{I} d\phi_1 \int_{-I}^{I} d\phi_2\ \rho(\phi_1,\phi_2)\left[k\mathrm{sn}\left(-\phi_1 - \frac{iI'}{3}\right)\mathrm{sn}\left(-\phi_1 - \frac{2iI'}{3}\right)\right]^j\left[k\mathrm{sn}(-\phi_1 - iI')\mathrm{sn}\left(-\phi_1 - \frac{4iI'}{3}\right)\right]^i \times\left[k\mathrm{sn}\left(-\phi_2 - \frac{iI'}{3}\right)\mathrm{sn}\left(-\phi_2 - \frac{2iI'}{3}\right)\right]^j\left[k\mathrm{sn}(-\phi_2 - iI')\mathrm{sn}\left(-\phi_2 - \frac{4iI'}{3}\right)\right]^i, \tag{A12}$$

with

$$\sinh K = \frac{i}{k\mathrm{sn}\left(\frac{2iI'}{3}\right)}, \tag{A13}$$

where we determine the function $\rho(\phi_1, \phi_2)$ from the distribution of the eigenvalues and the matrix elements [43]. Note that the next to minimal case with $(\nu, \nu') = (4, 8)$, that is, Eq. (2.9) reproduces Eq. (A12) by a suitable transformation.

We use the method of steepest descent for each integral to calculate the ACL. Repeating the same argument below Eq. (A10), we find that, if $\rho(\phi_1, \phi_2)$ is rewritten as $\rho(\phi_1 + \phi_2,\ \phi_1 - \phi_2)$, it has no $\phi_1 + \phi_2$ dependence: $\rho(\phi_1, \phi_2) = \rho(\phi_1 - \phi_2)$.

2. Passive rotations

We consider transfer matrices along various directions to find the role of C_{6v} symmetry. In Appendix A of Ref. [28], we defined the Ising model on a square lattice rotated through an arbitrary angle. We found that the lattice rotations shift the integration paths with their deformations. The same is expected to occur in lattice models with C_{6v}. However, exact calculations for C_{6v} symmetry are somewhat complicated: For the Kagomé lattice eight-vertex model, we can construct commuting transfer matrices along special directions [50,51,60]. Here, for the triangular lattice Ising model, we construct commuting transfer matrices along twelve directions to derive the three properties (i)–(iii). Note that commuting families have not been constructed so far for the Ising models on the Kagomé and diced lattices, which were investigated by the Pfaffian method; see, for example, Ref. [26].

We consider calculations of the ACLs. For example, above T_C ($\mu = 1$), we can estimate the integral in Eq. (A9) using the saddle-point method; see Sec. IV A. To calculate the correlation length along the horizontal direction $\theta = 0$, we take the $j \to \infty$ limit with $i = 0$ and then find the saddle point at $\phi_1 = -iI'/2 + I$; for the definition of θ, see Eq. (4.1). When θ increases as $\theta = n\pi/6$ with $n = 1, 2, \ldots, 5$, we find that the saddle point moves on the line $\Re(\phi_1) = I$; it is located at $\phi_1 = -iI'/2 - inI'/6 + I$.

The increase of θ corresponds to active rotations. Meanwhile, the method using passive rotations yields the same result. First, we consider the triangular lattice rotated clockwise by angle $n\pi/3$ ($n = 1, 2, \ldots, 5$). If we define the transfer matrix and shift operator on the rotated lattice, then they are identical to $\mathbf{Y}$ and $\mathbf{X}$, respectively. We repeat the analysis from Eq. (A1) to Eq. (A5); the limiting function is given by Eq. (A5) with ϕ_l replaced by $\bar{\phi}_l$ if we choose a suitable relation between them.

Above T_C, we rename ϕ_1 on the right-hand side of Eq. (A9) as $\bar{\phi}_1$. Comparing the saddle point on the $\bar{\phi}_1$ plane with that on the ϕ_1 plane, we find that ϕ_1 and $\bar{\phi}_1$ are related as $\bar{\phi}_1 = \phi_1 - inI'/3$. Note that

$$\begin{aligned} L_X\left(\phi_1 + \frac{iI'}{3}\right)^2 &= L_X(\phi_1) L_Y(\phi_1), \\ L_Y\left(\phi_1 + \frac{iI'}{3}\right)^2 &= L_X(\phi_1)^{-3} L_Y(\phi_1). \end{aligned} \tag{A14}$$

We extend these relations into the cases with $\mu > 1$, which indicates that $\bar{\phi}_l = \phi_l - inI'/3$ for all l. We find that the lattice rotation by $n\pi/3$ shifts the integration paths by $-inI'/3$ without deformations. In fact, for $T < T_C$, we start with Eq. (A12) with ϕ_1, ϕ_2 replaced by $\bar{\phi}_1, \bar{\phi}_2$. We obtain the same integration-path shifts caused by the $n\pi/3$-lattice rotations.

Second, to investigate the case $(2n-1)\pi/6$ ($n = 1, 2, \ldots, 6$), we define inhomogeneous transfer matrices as follows:

$$\begin{aligned} &[\tilde{\mathbf{V}}(u)]_{\sigma,\sigma'} \\ &\quad = \exp\left\{\sum_{l=0}^{N-1}\left[\varepsilon^{(0)}_{2l,2l} + \epsilon^{(1)}_{2l+1,2l} + \varepsilon^{(2)}_{2l+1,2l+1} + \epsilon^{(3)}_{2l+2,2l+1}\right]\right\}, \\ &[\tilde{\mathbf{W}}(u)]_{\sigma,\sigma'} \\ &\quad = \exp\left\{\sum_{l=0}^{N-1}\left[\epsilon^{(0)}_{2l,2l} + \varepsilon^{(1)}_{2l,2l+1} + \epsilon^{(2)}_{2l+1,2l+1} + \varepsilon^{(3)}_{2l+1,2l+2}\right]\right\}, \end{aligned} \tag{A15}$$

where $\sigma_{2N} = \sigma_0$ and $\sigma'_{2N} = \sigma'_0$. We denote local energies between σ_l and $\sigma'_{l'}$ with coupling constants $K(u)$, $K(u + v_0)$, $K(u + I' - v_0)$ and $K(u + v_0)$ [$K'(u)$, $K'(u + v_0)$, $K'(u + I' - v_0)$ and $K'(u + v_0)$] as $\epsilon^{(0)}_{l,l'}$, $\epsilon^{(1)}_{l,l'}$, $\epsilon^{(2)}_{l,l'}$ and $\epsilon^{(3)}_{l,l'}$ [$\varepsilon^{(0)}_{l,l'}$, $\varepsilon^{(1)}_{l,l'}$, $\varepsilon^{(2)}_{l,l'}$ and $\varepsilon^{(3)}_{l,l'}$], respectively. Then, the transfer matrix in the rotated system is given by

$$\tilde{\mathbf{Y}} = \lim_{\substack{u_1 \to v_0 \\ u_2 \to 0}} \frac{\tilde{\mathbf{W}}(u_1)}{\kappa(u_1 + I' - v_0)^{\frac{N}{2}}} \frac{\tilde{\mathbf{V}}(u_2)}{\kappa(u_2)^{\frac{N}{2}}}. \tag{A16}$$

We cannot construct the shift operator $\tilde{\mathbf{X}}$ in a similar manner. Despite this, we calculate the correlation length along the direction $(2n-1)\pi/6$ from the limiting functions corresponding to $\tilde{\mathbf{Y}}$ using the method of steepest descent. We find that the distances between the saddle points and integration paths change, which means that the lattice rotation by $(2n-1)\pi/6$ shifts the integration paths by $-i(2n-1)I'/6$.

As a result, the lattice rotation clockwise by $n\pi/6$ causes the integration paths to shift by $-inI'/6$ ($n = 1, 2, \ldots, 11$). The ACL calculated on the rotated lattice must be the same as that on the original lattice. We derive the equivalence with the help of the analyticity of the limiting functions (or eigenvalues). We find that (i) wide analyticity domains of the eigenvalues are required to ensure equivalence between the results in analyses along various directions. As shown in Eq. (A14), we find relations connected with the coordinate transformations for even n. The product structures of the sn functions in Eq. (A5) can derive the sixfold rotational symmetry. A necessary condition is that each of the limiting functions satisfies the inversion relation, that is, the first equation of Eq. (A27) or Eq. (A28) in Ref. [28]. Thus, (ii) the limiting functions should satisfy the equation corresponding to π-rotational symmetry. Note that if we assume (iii) doubly periodic structures, we obtain Eq. (A5). We expect that (iii) is generally satisfied for lattice systems; see Sec. II.

APPENDIX B: BIRATIONAL TRANSFORMATIONS

In this Appendix, we consider a relation between the algebraic curves (4.8) and (4.12); for the latter, see Sec. IV

of Ref. [28]. The set of α and β in Eq. (4.8) is a basis of an elliptic function field. Alternatively, the set of α and β in Eq. (4.12) is another example of a basis of the same elliptic function field. If this is the case, then the algebraic geometry indicates the possibility that rational functions relate to these two bases [52]. The relation is called a birational correspondence, and the two curves are considered to be birationally equivalent. We clarify a condition necessary for this possibility.

We start with the algebraic curve (4.12) found in the C_{4v} case:

$$\alpha'^2\beta'^2 + 1 + \bar{A}_2(\alpha'\beta' + 1)(\alpha' + \beta') + \alpha'^2 + \beta'^2 + \bar{A}_4\alpha'\beta' = 0. \tag{B1}$$

Using the sn functions, we parametrize Eq. (B1) as follows:

$$\alpha' = k\mathrm{sn}\left(\phi + b\frac{iI'}{4}\right)\mathrm{sn}\left(\phi - b\frac{iI'}{4}\right), \quad \beta' = k\mathrm{sn}\left(\phi + b\frac{iI'}{4} - \frac{iI'}{2}\right)\mathrm{sn}\left(\phi - b\frac{iI'}{4} - \frac{iI'}{2}\right), \tag{B2}$$

with

$$\bar{A}_2 = \frac{2\mathrm{cn}\left(b\frac{iI'}{2}\right)\mathrm{dn}\left(b\frac{iI'}{2}\right)}{1 + k\mathrm{sn}^2\left(b\frac{iI'}{2}\right)}, \qquad \bar{A}_4 = 4 - 4\frac{\left(k^{\frac{1}{2}} + k^{-\frac{1}{2}}\right)^2}{1 + k\mathrm{sn}^2\left(b\frac{iI'}{2}\right)}, \tag{B3}$$

where b is a free parameter introduced in Sec. III of Ref. [28]; also see the errata [66].

Equations (B1) and (4.8) are algebraic curves of genus 1. Furthermore, if both have the same modulus k, then we can relate them using rational functions as follows: Using the additional formula for Jacobi's elliptic functions, we obtain the first relation of Eq. (4.13):

$$\alpha' = \frac{\alpha + c}{1 + c\alpha}, \tag{B4}$$

where

$$c = -kS_+S_-, \quad S_\pm = \mathrm{sn}(v \pm \eta), \tag{B5}$$

with $v = biI'/4$ and $\eta = iI'/6$.

To find the second relation of Eq. (4.13), we define the following quantities:

$$\begin{aligned}
X_0 &= S_+^2 + S_-^2 - \mathrm{sn}^2(\eta) - \frac{c^2}{k^2\mathrm{sn}^2(\eta)},\\
X_1 &= S_+^2 + S_-^2 - c^2\mathrm{sn}^2(\eta) - \frac{1}{k^2\mathrm{sn}^2(\eta)},\\
X_2 &= \frac{1 - c^2}{k}[\mathrm{cn}(2v)\mathrm{dn}(2\eta) + \mathrm{dn}(2v)\mathrm{cn}(2\eta)] + 2c\left[\frac{\mathrm{cn}\,\mathrm{dn}}{k\mathrm{sn}}(\eta)\right]^2,\\
X_3 &= \frac{1 - c^2}{k}[\mathrm{cn}(2v)\mathrm{dn}(2\eta) + \mathrm{dn}(2v)\mathrm{cn}(2\eta)] - 2c\left[\frac{\mathrm{cn}\,\mathrm{dn}}{k\mathrm{sn}}(\eta)\right]^2,\\
X_4 &= 4S_+^2 + 4S_-^2 + 2(1 + c^2)\left[\frac{2\mathrm{cn}^2(\eta)\mathrm{dn}^2(\eta) - 1}{k^2\mathrm{sn}^2(\eta)} - \mathrm{sn}^2(\eta)\right].
\end{aligned} \tag{B6}$$

Then, we can prove that

$$X_0(\beta'^2\beta^2 + 1) + X_1(\beta'^2 + \beta^2) + X_2(\beta'\beta^2 + \beta') + X_3(\beta'^2\beta + \beta) + X_4\beta'\beta = 0. \tag{B7}$$

We multiply Eq. (B1) by $(X_0\beta^2 + X_1 + X_2\beta)$, and Eq. (B7) by $(\alpha'^2 + \bar{A}_2\alpha' + 1)$. We subtract the latter from the former. Then, it follows with the help of Eq. (B4) that

$$\beta' = \frac{\Phi_1(\alpha, \beta)}{\Phi_2(\alpha, \beta)}, \tag{B8}$$

where $\Phi_1(\alpha, \beta)$ and $\Phi_2(\alpha, \beta)$ are the polynomials of α and β given by

$$\begin{aligned}
\Phi_1(\alpha, \beta) &= (X_1 - X_0)\{(c^2 + \bar{A}_2c + 1)(\alpha^2 + 1) + [\bar{A}_2(c^2 + 1) + 4c]\alpha\}(\beta^2 - 1),\\
\Phi_2(\alpha, \beta) &= \{[\bar{A}_2(c^2 + 1) + \bar{A}_4c](\alpha^2 + 1) + [\bar{A}_4(c^2 + 1) + 4\bar{A}_2c]\alpha\}(X_0\beta^2 + X_3\beta + X_1)\\
&\quad - \{(c^2 + \bar{A}_2c + 1)(\alpha^2 + 1) + [\bar{A}_2(c^2 + 1) + 4c]\alpha\}(X_2\beta^2 + X_4\beta + X_2).
\end{aligned} \tag{B9}$$

We derive the inverse transformation similarly: From Eq. (B4) we obtain

$$\alpha = \frac{\alpha' - c}{1 - c\alpha'}. \tag{B10}$$

We use Eq. (4.8) instead of Eq. (B1). It follows that

$$\beta = \frac{\Psi_1(\alpha', \beta')}{\Psi_2(\alpha', \beta')}, \tag{B11}$$

where $\Psi_1(\alpha', \beta')$ and $\Psi_2(\alpha', \beta')$ are the fourth-order polynomials of α' and β' given by

$$\begin{aligned}
\Psi_1(\alpha', \beta') &= (1-c)(\alpha'+1)[(c\alpha'-1)(X_0\beta'^2 + X_2\beta' + X_1) + (\alpha'-c)(X_1\beta'^2 + X_2\beta' + X_0)], \\
\Psi_2(\alpha', \beta') &= \{(c^2 - cH + 1)(\alpha'^2 + 1) + [(c^2+1)H - 4c]\alpha'\}(X_0\beta'^2 + X_2\beta' + X_1) \\
&\quad + (c-1)(\alpha'+1)(\alpha'-c)(X_3\beta'^2 + X_4\beta' + X_3).
\end{aligned} \tag{B12}$$

Consequently, we obtain the birational transformation that connects the algebraic curves (1.10) and (4.12) [52].

[1] G. Wulff, Z. Kristallogr. Cryst. Mater. **34**, 449 (1901).
[2] M. von Laue, Z. Kristallogr. **105**, 124 (1944).
[3] C. Herring, Phys. Rev. **82**, 87 (1951).
[4] W. K. Burton, N. Cabrera, and F. C. Frank, Philos. Trans. R. Soc. London, Ser. A **243**, 299 (1951).
[5] D. B. Abraham and P. Reed, Phys. Rev. Lett. **33**, 377 (1974).
[6] D. B. Abraham and P. Reed, Commun. Math. Phys. **49**, 35 (1976).
[7] H. van Beijeren, Phys. Rev. Lett. **38**, 993 (1977).
[8] C. Jayaprakash, W. F. Saam, and S. Teitel, Phys. Rev. Lett. **50**, 2017 (1983).
[9] C. Rottman and M. Wortis, Phys. Rev. B **24**, 6274 (1981).
[10] J. E. Avron, H. van Beijeren, L. S. Schulman, and R. K. P. Zia, J. Phys. A: Math. Gen. **15**, L81 (1982).
[11] R. K. P. Zia and J. E. Avron, Phys. Rev. B **25**, 2042 (1982).
[12] E. M. Lieb and F. Y. Wu, Two-dimensional ferroelectric models, in *Phase Transitions and Critical Phenomena*, edited by C. Domb and M. S.Green (Academic Press, London, 1972), Vol. 1, pp. 332–490.
[13] R. Baxter, *Exactly Solved Models in Statistical Mechanics*, Dover books on physics (Dover Publications, Mineola, NY, 2007).
[14] L. D. Landau and E. M. Lifshitz, *Statistical Physics, Part 1*, 3rd ed. (Butterworth Heinemann, Oxford, UK, 1980), Vol. 5.
[15] A. F. Andreev, Sov. Phys. JETP **53**, 1063 (1981).
[16] Y. Akutsu and N. Akutsu, Phys. Rev. Lett. **64**, 1189 (1990).
[17] W. Selke and W. Pesch, Z. Phys. B **47**, 335 (1982).
[18] M. Fujimoto, J. Stat. Phys. **67**, 123 (1992).
[19] M. Fujimoto, J. Phys. A: Math. Gen. **26**, 2285 (1993).
[20] M. Fujimoto, J. Phys. A: Math. Gen. **30**, 3779 (1997).
[21] N. Akutsu and Y. Akutsu, J. Phys. Soc. Jpn. **56**, 2248 (1987).
[22] Y. Akutsu and N. Akutsu, J. Phys. Soc. Jpn. **56**, 9 (1987).
[23] M. Holzer and M. Wortis, Phys. Rev. B **40**, 11044 (1989).
[24] R. K. P. Zia, Phys. Lett. A **64**, 345 (1978).
[25] M. Holzer, Phys. Rev. Lett. **64**, 653 (1990).
[26] M. Holzer, Phys. Rev. B **42**, 10570 (1990).
[27] M. Hamermesh, *Group Theory and Its Application to Physical Problems* (Dover, Mineola, NY, 1989).
[28] M. Fujimoto and H. Otsuka, Phys. Rev. E **102**, 032141 (2020).
[29] H. N. V. Temperley, E. H. Lieb, and S. F. Edwards, Proc. R. Soc. London A **322**, 251 (1971).
[30] R. J. Baxter, J. Phys. C: Solid State Phys. **6**, L445 (1973).
[31] F. Y. Wu, Rev. Mod. Phys. **54**, 235 (1982).
[32] A. Klümper, A. Schadschneider, and J. Zittartz, Z. Phys. B **76**, 247 (1989).
[33] E Buddenoir and S. Wallon, J. Phys. A: Math. Gen. **26**, 3045 (1993).
[34] M. Fujimoto, J. Stat. Phys. **59**, 1355 (1990).
[35] M. Fujimoto, J. Stat. Phys. **61**, 1295 (1990).
[36] A. Klümper, Int. J. Mod. Phys. B **04**, 871 (1990).
[37] H. Cheng and T. T. Wu, Phys. Rev. **164**, 719 (1967).
[38] B. M. McCoy and T. T. Wu, *The Two-Dimensional Ising Model* (Harvard University Press, Cambridge, MA, 2013).
[39] K. Yamada, Prog. Theor. Phys. **69**, 1295 (1983).
[40] K. Yamada, Prog. Theor. Phys. **71**, 1416 (1984).
[41] K. Yamada, Prog. Theor. Phys. **72**, 922 (1984).
[42] K. Yamada, Prog. Theor. Phys. **76**, 602 (1986).
[43] J. D. Johnson, S. Krinsky, and B. M. McCoy, Phys. Rev. A **8**, 2526 (1973).
[44] L. Laanait, Phys. Lett. A **124**, 480 (1987).
[45] M. Fujimoto, Physica A **233**, 485 (1996).
[46] H. G. Vaidya, Phys. Lett. A **57**, 1 (1976).
[47] J. Stephenson, J. Math. Phys. **5**, 1009 (1964).
[48] Y. Chan, A. J. Guttmann, B. G. Nickel, and J. H. H. Perk, J. Stat. Phys. **145**, 549 (2011), and the references therein.
[49] R. K. P. Zia, J. Stat. Phys. **45**, 801 (1986).
[50] M. Fujimoto, J. Stat. Phys. **90**, 363 (1998).
[51] M. Fujimoto, Physica A **264**, 149 (1999).
[52] R. J. Walker, *Algebraic Curves* (Princeton University Press, Princeton, NJ, 1950), Vol. 13.
[53] M. Fujimoto, J. Phys. A: Math. Gen. **35**, 7553 (2002).
[54] R. H. Swendsen and J.-S. Wang, Phys. Rev. Lett. **58**, 86 (1987).
[55] U. Wolff, Phys. Rev. Lett. **60**, 1461 (1988).
[56] U. Wolff, Phys. Rev. Lett. **62**, 361 (1989).
[57] H. G. Evertz and W. von der Linden, Phys. Rev. Lett. **86**, 5164 (2001).
[58] C. M. Fortuin and P. W. Kasteleyn, Physica **57**, 536 (1972).
[59] M. Suzuki, Prog. Theor. Phys. **51**, 1992 (1974).

[60] M. Fujimoto, J. Phys. A: Math. Gen. **35**, 1517 (2002).
[61] M. Namba, *Geometry of Projective Algebraic Curves*, Monographs and textbooks in pure and applied mathematics (M. Dekker, New York, NY, 1984).
[62] J. M. Kosterlitz and D. J. Thouless, J. Phys. C **6**, 1181 (1973).
[63] J. M. Kosterlitz, J. Phys. C **7**, 1046 (1974).
[64] F. Y. Wu, Phys. Rev. **168**, 539 (1968).
[65] R. J. Baxter, Philos. Trans. R. Soc. London A **289**, 315 (1978).
[66] M. Fujimoto and H. Otsuka, Phys. Rev. E **105**, 059904(E) (2022).